

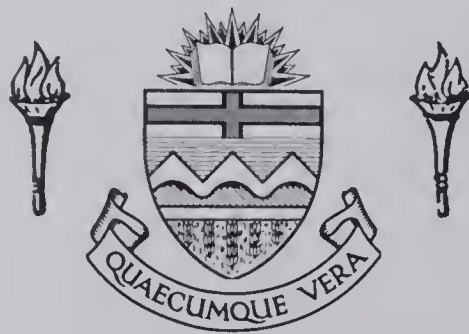
For Reference

NOT TO BE TAKEN FROM THIS ROOM

For Reference

NOT TO BE TAKEN FROM THIS ROOM

Ex LIBRIS
UNIVERSITATIS
ALBERTAENSIS



UNIVERSITY OF ALBERTA
LIBRARY

Regulations Regarding Theses and Dissertations

Typescript copies of theses and dissertations for Master's and Doctor's degrees deposited in the University of Alberta Library, as the official Copy of the Faculty of Graduate Studies, may be consulted in the Reference Reading Room only.

A second copy is on deposit in the Department under whose supervision the work was done. Some Departments are willing to loan their copy to libraries, through the inter-library loan service of the University of Alberta Library.

These theses and dissertations are to be used only with due regard to the rights of the author. Written permission of the author and of the Department must be obtained through the University of Alberta Library when extended passages are copied. When permission has been granted, acknowledgement must appear in the published work.


This thesis or dissertation has been used in accordance with the above regulations by the persons listed below. The borrowing library is obligated to secure the signature of each user.

Please sign below:

THE UNIVERSITY OF ALBERTA

NUMERICAL SOLUTION FOR COMBINED FREE AND FORCED LAMINAR
CONVECTION IN HORIZONTAL RECTANGULAR CHANNELS

by

GUANG-JYH HWANG, B.Sc. 
(National Taiwan University)

A THESIS

SUBMITTED TO THE FACULTY OF GRADUATE STUDIES
IN PARTIAL FULFILMENT OF THE REQUIREMENTS FOR THE DEGREE
OF MASTER OF SCIENCE

DEPARTMENT OF MECHANICAL ENGINEERING

EDMONTON, ALBERTA

April, 1968



Digitized by the Internet Archive
in 2019 with funding from
University of Alberta Libraries

<https://archive.org/details/Hwang1968>

UNIVERSITY OF ALBERTA
FACULTY OF GRADUATE STUDIES

The undersigned certify that they have read, and recommend to the Faculty of Graduate Studies for acceptance, a thesis entitled "NUMERICAL SOLUTION FOR COMBINED FREE AND FORCED LAMINAR CONVECTION IN HORIZONTAL RECTANGULAR CHANNELS" submitted by GUANG-JYH HWANG in partial fulfilment of the requirements for the degree of Master of Science.

ABSTRACT

Combined free and forced convection for steady fully developed laminar flow in long horizontal rectangular channels under the thermal boundary conditions of constant axial temperature gradient and peripherally uniform wall temperature at any axial position is approached by the method of successive-overrelaxation. Two vortices (secondary flow) with opposite sense are observed in a cross section normal to the main flow as a result of the buoyancy effect. The convergence of the numerical solution is ascertained. Graphical results are presented for velocity and temperature distributions, streamlines, isotherms, \bar{w}/\bar{w}_0 vs. $ReRa$, $fRe/(fRe)_0$ vs. $ReRa$ and Nu/Nu_0 vs. $ReRa$ for the aspect ratios $\gamma = 0.2, 0.5, 1, 2$ and 5 and $Pr = 0.73$. For a square channel, the heat transfer result for $Pr = 7.2$ is also presented.

ACKNOWLEDGEMENTS

The author wishes to extend his appreciation to

- Dr. K.C. Cheng for his supervision of this thesis,
- Dr. G.S.H. Lock and Dr. W. Nakayama for their valuable suggestions,
- The members of the Computing Science Department for their advice and cooperation in computer programming,
- Miss H. Wozniuk for her patience in typing this thesis,
- The National Research Council of Canada for studentship,
- My parents and wife for their constant encouragement.

TABLE OF CONTENTS

	<u>Page</u>
CHAPTER I <u>INTRODUCTION</u>	1
CHAPTER II <u>THEORETICAL ANALYSIS</u>	3
2.1 Governing Equations and Boundary Conditions.	3
2.2 Non-Dimensional Transformations	5
CHAPTER III <u>FINITE-DIFFERENCE APPROXIMATION</u>	8
3.1 Finite-Difference Equations	8
3.2 Method of Solution	14
(a) Iterative Procedure	14
(b) Errors and Determination of Mesh Size	15
CHAPTER IV <u>RESULTS AND DISCUSSION</u>	18
4.1 Flow and Heat Transfer Characteristics	18
4.2 ReRa Number Effects	20
4.3 Aspect Ratio Effects	21
4.4 Results of \bar{w}/\bar{w}_0 , $fRe/(fRe)_0$, Nu/Nu_0 and Pr Number Effects	23
4.5 Conclusions	24
<u>REFERENCES</u>	27
APPENDIX A NORMALIZATION OF EQUATIONS	30
APPENDIX B METHOD OF SOLVING EQUATIONS $\nabla^2 f = F$ and $\nabla^4 f = F'$	33
APPENDIX C PERTURBATION METHOD	36
APPENDIX D FORTRAN PROGRAMMING	38

LIST OF FIGURES

<u>FIGURE</u>		<u>Page</u>
1	Coordinate system and finite-difference network for a rectangular channel	45
2	Effect of grid size on flow and heat transfer results for square channel $\gamma = 1$ with $Pr = 0.73$ and $ReRa = 0$ and 1.386×10^4	46
3	Dimensionless axial velocity distribution at $X = a/2$ with $ReRa$ as a parameter in a square channel $\gamma = 1$ and $Pr = 0.73$	47
4	Dimensionless temperature distribution at $X = a/2$ with $ReRa$ as a parameter in a square channel $\gamma = 1$ and $Pr = 0.73$	48
5	Dimensionless axial velocity and temperature distributions at $Y = b/2$ with $ReRa$ as a parameter in a square channel $\gamma = 1$ and $Pr = 0.73$	49
6	Streamlines and isothermals for a square channel $\gamma = 1$ with $Pr = 0.73$ and $ReRa = 1.030 \times 10^5$	50
7	Dimensionless axial velocity distribution at $X = a/2$ with $ReRa$ as a parameter in a rectangular channel $\gamma = 2$ and $Pr = 0.73$	51
8	Dimensionless temperature distribution at $X = a/2$ with $ReRa$ as a parameter in a rectangular channel $\gamma = 2$ and $Pr = 0.73$	52

<u>FIGURE</u>		<u>Page</u>
9	Dimensionless axial velocity and temperature distributions at $Y = b/2$ with $ReRa$ as a parameter in a rectangular channel $\gamma = 2$ and $Pr = 0.73$	53
10	Streamlines and isothermals for a rectangular channel $\gamma = 2$ with $Pr = 0.73$ and $ReRa = 1.408 \times 10^5$	54
11	Dimensionless axial velocity distribution at $X = a/2$ with $ReRa$ as a parameter in a rectangular channel $\gamma = 5$ and $Pr = 0.73$	55
12	Dimensionless temperature distribution at $X = a/2$ with $ReRa$ as a parameter in a rectangular channel $\gamma = 5$ and $Pr = 0.73$	56
13	Dimensionless axial velocity and temperature distributions at $Y = b/2$ with $ReRa$ as a parameter in a rectangular channel $\gamma = 5$ and $Pr = 0.73$	57
14	Streamlines and isothermals for a rectangular channel $\gamma = 5$ with $Pr = 0.73$ and $ReRa = 2.984 \times 10^5$	58
15	Dimensionless axial velocity distribution at $X = a/2$ with $ReRa$ as a parameter in a rectangular channel $\gamma = 0.5$ and $Pr = 0.73$	59
16	Dimensionless temperature distribution at $X = a/2$ with $ReRa$ as a parameter in a rectangular channel $\gamma = 0.5$ and $Pr = 0.73$	60
17	Dimensionless axial velocity and temperature distributions at $Y = b/2$ with $ReRa$ as a parameter in a rectangular channel $\gamma = 0.5$ and $Pr = 0.73$	61

<u>FIGURE</u>		<u>Page</u>
18	Streamlines and isothermals for a rectangular channel $\gamma = 0.5$ with $Pr = 0.73$ and $ReRa = 1.381 \times 10^5$	62
19	Dimensionless axial velocity distributions at $X = a/2$ with $ReRa$ as a parameter in a rectangular channel $\gamma = 0.2$ and $Pr = 0.73$	63
20	Dimensionless temperature distribution at $X = a/2$ with $ReRa$ as a parameter in a rectangular channel $\gamma = 0.2$ and $Pr = 0.73$	64
21	Dimensionless axial velocity and temperature distri- butions at $Y = b/2$ with $ReRa$ as a parameter in a rec- tangular channel $\gamma = 0.2$ and $Pr = 0.73$	65
22	Streamlines and isothermals for a rectangular channel $\gamma = 0.2$ with $Pr = 0.73$ and $ReRa = 2.535 \times 10^5$	66
23	$\overline{w}/\overline{w}_0$ versus $ReRa$ with aspect ratio γ as a parameter ..	67
24	$f Re/(f Re)_0$ versus $ReRa$ with aspect ratio γ as a parameter	68
25	Nu/Nu_0 versus $ReRa$ with aspect ratio γ as a parameter.	69

LIST OF TABLES

<u>TABLE</u>		<u>Page</u>
1	Numerical results for square channel $\gamma = 1$ and Pr = 0.73	70
2	Numerical results for square channel $\gamma = 1$ and Pr = 7.3	71
3	Numerical results for aspect ratio $\gamma = 2$ and Pr = 0.73	72
4	Numerical results for aspect ratio $\gamma = 5$ and Pr = 0.73	73
5	Numerical results for aspect ratio $\gamma = 0.5$ and Pr = 0.73	74
6	Numerical results for aspect ratio $\gamma = 0.2$ and Pr = 0.73	75
7	Comparison of Nusselt number with exact value for ReRa = 0	76
8	Numerical results of $\overline{(\frac{\partial w}{\partial n})_W}$, $ \overline{\frac{\partial \theta}{\partial n}} _W$ and $\overline{w}/4$ for Pr = 0.73	76

NOMENCLATURE

A	= cross-sectional area
A_i	= constant
a	= width of a rectangular channel
B_1	= constant, $2(1/h^2 + 1/\ell^2)$
B_2	= constant, $1/n^2$
B_3	= constant, $1/\ell^2$
b	= height of a rectangular channel
C	= constant, $-C_1 D_e^3 / 4\nu\mu = Re/\bar{w}$
C_1	= axial pressure gradient, $\partial P_0 / \partial Z$
C_2	= axial temperature gradient, $\partial T / \partial Z$
D_e	= equivalent hydraulic diameter, $4A/S$
Ec	= Eckert number $\bar{w}^2 / C_p C_2 D_e$
f	= friction factor, $2\bar{T}_w / (\rho \bar{w}^2)$, or a function of X and Y
F, F', G	= functions of X and Y
Gr	= Grashof number, $\beta g C_2 D_e^4 / \nu^2$
g	= gravitational acceleration
h	= dimensionless grid spacing in the X direction, $(r+1)/4M$
\bar{h}	= average heat transfer coefficient, $-\bar{q}/T_M$
K	= thermal conductivity
L	= axial direction characteristic length
ℓ	= dimensionless grid spacing in the Y direction, $(r+1)/(2\gamma N)$

M	= number of divisions in the X direction
N	= number of divisions in the Y direction
Nu	= Nusselt number, $\bar{h}D_e/K$
n	= dimensionless inward-drawn normal or nth iteration for superscript
n'	= dimensional inward-drawn normal
Os	= Ostrach number, $\beta g D_e / C_p$
P	= pressure
P'	= pressure deviation which is a function of X and Y
P ₀	= axial pressure distribution measured on the bottom plate Y = 0, $0 \leq x \leq a$ and a function of z only
P _w	= pressure at wall, $P_0(z) - P_w g Y$
Pr	= Prandtl number, ν/α
Ra	= Rayleigh number, $\beta g C_2 D_e^4 / \nu \alpha$
Re	= Reynolds number, $D_e \bar{W} / \nu$
S	= circumference of cross-section
T	= local temperature
T _M	= mixed mean temperature difference
T _w	= wall temperature
U,V,W	= velocity components in X, Y and Z directions
u,v,w	= dimensionless velocity components in X, Y and Z directions or normalized velocity components defined in (A.1)
X,Y,Z	= rectangular coordinates
x,y,z	= dimensionless rectangular coordinates

GREEK LETTERS

α	= thermal diffusivity
β	= coefficient of thermal expansion
γ	= aspect ratio of a rectangular channel, a/b
ξ	= vorticity defined in (A.3)
ε	= a prescribed small number
ε_i	= small quantities, $i = 1, 2, \dots, 5$ Defined in (A.4)
θ	= dimensionless temperature difference, $(T - T_W)/(C_2 D_e \text{Pr } C)$ or normalized temperature difference, $(T - T_W)/C_2 D_e$
μ	= viscosity
$\bar{\mu}$	= a value defined in equation (A.8)
ν	= kinematic viscosity
ρ	= density
$\bar{\tau}_W$	= mean shearing stress at wall
Ψ	= dimensionless stream function
$\hat{\omega}$	= relaxation factor
∇_1^2	= Laplacian operator
∇^2	= dimensionless Laplacian operator

SUBSCRIPTS

c	= characteristic quantity
i, j	= space subscripts of grid point in X and Y directions
0	= condition for pure forced convection
W	= the value at wall

CHAPTER I

INTRODUCTION

The significant effects of body forces on forced convective heat transfer in internal flows have been studied by many investigators in recent years. Morton [1] analysed the buoyancy effects for fully developed laminar forced convection in uniformly heated horizontal tubes at low Rayleigh numbers by a perturbation method. His analysis cannot be readily extended to the cases with large Rayleigh numbers. The same problem without the assumption of a constant axial pressure gradient was discussed by del Casal and Gill [2] using a perturbation analysis. A theoretical investigation of natural convection effects in fully developed horizontal flow between infinite parallel plates with a linear axial temperature distribution was presented also by Gill and de Casal [3]. Mori and Futagami [4] reported an analytical study for fully developed forced convective heat transfer in uniformly heated horizontal tubes with strong secondary flow caused by buoyancy forces using boundary layer approximation. Mori and his co-workers [5] also carried out an experimental study and verified the result of theoretical analysis. The influence of tube orientation on combined free and forced fully developed laminar convection heat transfer was discussed by Iqbal and Stachiewicz [6] using a perturbation approach similar to Morton's [1]. Recently, an experimental

investigation on combined free and forced convection in a horizontal circular tube was reported by McComas and Eckert [7] with several earlier experimental investigations quoted in the references.

It is noted that previous theoretical studies on combined free and forced convection in horizontal channel flow are largely confined to circular pipes. In contrast, several analytical methods are available in the literature for combined forced and free convection in vertical channels of various geometrical shapes. For example, combined forced and free convection for fully developed laminar flow in vertical rectangular channels of constant axial wall temperature gradient with uniform internal heat generation was treated by Han [8] using double Fourier series. Tao [9] approached the same problem by introducing a complex function relating to the velocity and temperature fields.

The purpose of this thesis is to present flow and heat transfer results for fully developed laminar forced convection with helical paths of fluid particles due to the buoyancy effects in long horizontal rectangular channels having aspect ratios 0.2, 0.5, 1, 2 and 5 by successive-overrelaxation method [10]. In this study, the wall temperature is considered to be peripherally invariant and a linear function of axial position.

Secondary flow for convective heat transfer in various ducts is also known to occur through such body forces as centrifugal and coriolis forces. Many such investigations are available in the literature [11-15].

CHAPTER II

THEORETICAL ANALYSIS

2.1 Governing Equations and Boundary Conditions

Consider the steady incompressible fully developed laminar flow in a uniformly heated horizontal rectangular channel with peripherally uniform wall temperature at any axial position. The motion will be referred to Cartesian coordinate (X,Y,Z) as shown in Fig. 1. It will be assumed that the effects of viscous dissipation ($0 \leq \text{Pr} \ll 1$ and $\text{Ec} \ll 1$) and of compression work in the energy equation can be neglected, that variations in density due to temperature changes are so small that they need to be taken into account only in the buoyancy term, and that the kinematic viscosity ν , and the thermal conductivity, K , can be taken as constants. With the above assumptions, the governing equations are (see APPENDIX A):

Continuity Equation

$$\frac{\partial U}{\partial X} + \frac{\partial V}{\partial Y} = 0 \quad (1)$$

Momentum Equations

$$U \frac{\partial U}{\partial X} + V \frac{\partial U}{\partial Y} = - \frac{1}{\rho} \frac{\partial P'}{\partial X} + \nu \nabla_1^2 U \quad (2)$$

$$U \frac{\partial V}{\partial X} + V \frac{\partial V}{\partial Y} = - \frac{1}{\rho} \frac{\partial P'}{\partial Y} + \nu \nabla_1^2 V + \beta g (T - T_W) \quad (3)$$

$$U \frac{\partial W}{\partial X} + V \frac{\partial W}{\partial Y} = - \frac{1}{\rho} \frac{\partial P_0}{\partial Z} + \nu \nabla_1^2 W \quad (4)$$

It is noted here that $\partial W / \partial Z = 0$, $\partial U / \partial Z = 0$ and $\partial V / \partial Z = 0$ follow from the assumption of steady fully developed flow.

Energy equation

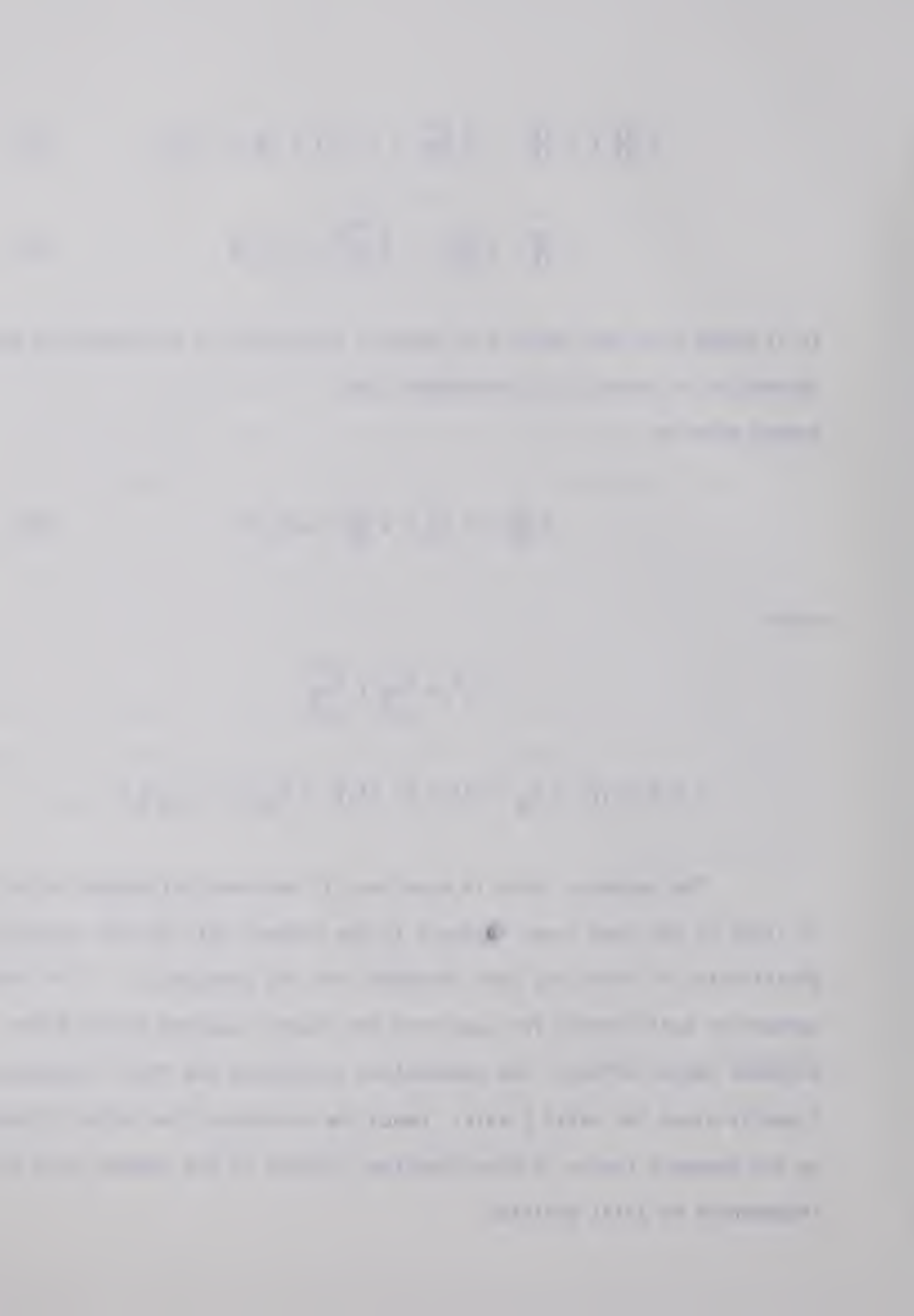
$$U \frac{\partial T}{\partial X} + V \frac{\partial T}{\partial Y} + W \frac{\partial T}{\partial Z} = \alpha \nabla_1^2 T \quad (5)$$

where

$$\nabla_1^2 = \frac{\partial^2}{\partial X^2} + \frac{\partial^2}{\partial Y^2}$$

$$P = P'(X, Y) + P_W(Y, Z) = P'(X, Y) + P_0(Z) - \rho_W g Y$$

The buoyancy force in equation (3) has been calculated relative to fluid at the same level adjacent to the channel wall and the remaining distribution of force has been adsorbed into the pressure, P' . For steady convection sufficiently far away from the channel opening to avoid the entrance length effects, the temperature throughout the fluid increases linearly along the axial Z axis. Hence the secondary flow motion driven by the buoyancy forces in cross-sections normal to the channel axis is independent of axial position.



The boundary conditions are

$$U = V = W = T - T_W = P' = 0 \text{ at channel wall.}$$

2.2 Non-Dimensional Transformations

For the purposes of simplification and analysis, the above equations (1 - 5) may be reduced to non-dimensional form by the following transformations.

$$X = D_e x, \quad Y = D_e y$$

$$U = (\nu/D_e)u, \quad V = (\nu/D_e)v, \quad W = (\nu C/D_e)w,$$

$$\partial P_0 / \partial Z = C_1, \quad \partial T / \partial Z = C_2$$

$$C = -C_1 D_e^3 / 4\nu\mu, \quad T - T_W = (C_2 D_e \text{Pr} C)\theta$$

$$\text{Re} = \bar{W} D_e / \nu = C \bar{w} \quad (6)$$

and a dimensionless stream function ψ ,

$$u = \partial\psi/\partial y, \quad v = -\partial\psi/\partial x \quad (7)$$

The momentum and energy equations can be written in dimension-

less form as follows after eliminating pressure terms between equations (2) and (3), and applying the above transformations.

$$\frac{\partial \psi}{\partial y} \frac{\partial}{\partial x} \nabla^2 \psi - \frac{\partial \psi}{\partial x} \frac{\partial}{\partial y} \nabla^2 \psi = \nabla^2 \nabla^2 \psi - Ra C \frac{\partial \theta}{\partial x} \quad (8)$$

$$\frac{\partial \psi}{\partial y} \frac{\partial w}{\partial x} - \frac{\partial \psi}{\partial x} \frac{\partial w}{\partial y} = \nabla^2 w + 4 \quad (9)$$

$$Pr \left(\frac{\partial \psi}{\partial y} \frac{\partial \theta}{\partial x} - \frac{\partial \psi}{\partial x} \frac{\partial \theta}{\partial y} \right) = \nabla^2 \theta - w \quad (10)$$

Although the partial differential equations become fourth order, the 5 unknowns U, V, W, P', T in equation (1-5) are now reduced to 3 unknowns ψ, w, θ . And because of symmetry, it is only required to consider half of the rectangular region. Consequently, the boundary conditions can be rewritten as:

$$\frac{\partial \psi}{\partial x} = \frac{\partial \psi}{\partial y} = w = \theta = 0 \text{ at channel wall}$$

$$\frac{\partial \psi}{\partial y} = \frac{\partial^2 \psi}{\partial x^2} = \frac{\partial w}{\partial x} = \frac{\partial \theta}{\partial x} = 0 \text{ at } X = a/2, 0 < Y < b \quad (11)$$

Solution of equations (8 - 10) satisfying the boundary conditions (11) is a matter of considerable mathematical difficulty. Morton [1] employed a perturbation method for the solution of the corresponding three

equations and the associated boundary conditions for circular pipes. In this study for rectangular channels, a point iterative method [10] is used.

CHAPTER III

FINITE-DIFFERENCE APPROXIMATION

3.1 Finite-Difference Equations

The above equations (9) and (10) can be regarded as having the form

$$\frac{\partial^2 f}{\partial x^2} + \frac{\partial^2 f}{\partial y^2} = F(x,y) \quad (12)$$

which is called Poisson's (or inhomogeneous harmonic) equation and its finite-difference approximation is [10]

$$\begin{aligned} f_{i,j} \approx & \frac{\ell^2}{2(h^2 + \ell^2)} (f_{i+1,j} + f_{i-1,j}) + \frac{h^2}{2(h^2 + \ell^2)} (f_{i,j+1} + f_{i,j-1}) \\ & - \frac{h^2 \ell^2}{2(h^2 + \ell^2)} F(x,y) \end{aligned} \quad (13)$$

The inhomogeneous term $F(x,y)$ in equation (9) can be approximated as:

$$\begin{aligned} F(x,y) &= \frac{\partial \psi}{\partial y} \frac{\partial w}{\partial x} - \frac{\partial \psi}{\partial x} \frac{\partial w}{\partial y} - 4 \\ &\approx \frac{\partial \psi_{i,j}}{\partial y} \frac{w_{i+1,j} - w_{i-1,j}}{2h} - \frac{\partial \psi_{i,j}}{\partial x} \frac{w_{i,j+1} - w_{i,j-1}}{2\ell} - 4 \end{aligned}$$

or

$$F(x,y) \approx u_{i,j} \frac{w_{i+1,j} - w_{i-1,j}}{2h} + v_{i,j} \frac{w_{i,j+1} - w_{i,j-1}}{2\ell} - 4 \quad (14)$$

Using the above approximations, the finite-difference equation for equation (9) becomes,

$$\begin{aligned} w_{i,j} \approx & \left[\frac{\ell^2}{2} (w_{i+1,j} + w_{i-1,j}) + \frac{h^2}{2} (w_{i,j+1} + w_{i,j-1}) \right. \\ & - \frac{h\ell^2}{4} u_{i,j} (w_{i+1,j} - w_{i-1,j}) - \frac{h^2\ell}{4} v_{i,j} (w_{i,j+1} - w_{i,j-1}) \\ & \left. + 2h^2\ell^2 \right] / (h^2 + \ell^2) \end{aligned} \quad (15)$$

Similarly, equation (10) becomes

$$\begin{aligned} \theta_{i,j} \approx & \left[\frac{\ell^2}{2} (\theta_{i+1,j} + \theta_{i-1,j}) + \frac{h^2}{2} (\theta_{i,j+1} + \theta_{i,j-1}) \right. \\ & - \frac{h\ell^2}{4} \text{Pr } u_{i,j} (\theta_{i+1,j} - \theta_{i-1,j}) - \frac{h^2\ell}{4} \text{Pr } v_{i,j} (\theta_{i,j+1} - \theta_{i,j-1}) \\ & \left. - w_{i,j} \frac{h^2\ell^2}{2} \right] / (h^2 + \ell^2) \end{aligned} \quad (16)$$

Equation (8) can be considered as inhomogeneous biharmonic equation which has the form

$$\nabla^2 \nabla^2 f = F'(x,y)$$

or

$$\nabla^2 G = F(x,y)$$

$$\nabla^2 f = G$$

Its finite-difference approximation can be written down by double application of approximation (13). Then equation (8) can be approximated by

$$\begin{aligned} \psi_{i,j} \approx & [2B_1 B_2 (\psi_{i+1,j} + \psi_{i-1,j}) + 2B_1 B_3 (\psi_{i,j+1} + \psi_{i,j-1}) \\ & - B_2^2 (\psi_{i+2,j} + \psi_{i-2,j}) - B_3^2 (\psi_{i,j+2} + \psi_{i,j-2}) \\ & - 2B_2 B_3 (\psi_{i+1,j+1} + \psi_{i-1,j+1} + \psi_{i-1,j-1} + \psi_{i+1,j-1}) \\ & + \frac{U_{i,j}}{2h} \{B_1 (\psi_{i-1,j} - \psi_{i+1,j}) + B_2 (\psi_{i+2,j} - \psi_{i-2,j}) \\ & + B_3 (\psi_{i+1,j+1} + \psi_{i+1,j-1} - \psi_{i-1,j+1} - \psi_{i-1,j-1})\} \\ & + \frac{V_{i,j}}{2\ell} \{B_1 (\psi_{i,j-1} - \psi_{i,j+1}) + B_3 (\psi_{i,j+2} - \psi_{i,j-2}) \} \end{aligned}$$

$$\begin{aligned}
& + B_2 (\psi_{i+1,j+1} + \psi_{i-1,j+1} - \psi_{i-1,j-1} - \psi_{i+1,j-1}) \} \\
& + Ra C \frac{\partial \theta_{i,j}}{\partial x}] / (B_1^2 + 2B_2^2 + 2B_3^2) \quad (17)
\end{aligned}$$

where

$$B_1 = 2(B_2 + B_3), \quad B_2 = 1/h^2, \quad B_3 = 1/\ell^2$$

$$\partial \theta_{i,j} / \partial x \approx (\theta_{i-2,j} - 8\theta_{i-1,j} + 8\theta_{i+1,j} - \theta_{i+2,j}) / 12h$$

One notes that the finite-difference approximations for the secondary flow velocity components u and v are as follows:

$$j = 2, \quad u_{i,2} \approx (\psi_{i,5} - 6\psi_{i,4} + 18\psi_{i,3} - 10\psi_{i,2}) / 12\ell \quad (18)$$

$$j = 3, 4, \dots, N - 1,$$

$$u_{i,j} \approx (\psi_{i,j-2} - 8\psi_{i,j-1} + 8\psi_{i,j+1} - \psi_{i,j+2}) / 12\ell \quad (19)$$

$$j = N \quad u_{i,N} \approx (\psi_{i,N-3} - 6\psi_{i,N-2} + 18\psi_{i,N-1} - 10\psi_{i,N}) / (-12\ell) \quad (20)$$

where

$$i = 2, 3, \dots, M + 1$$

$$i = 2, \quad v_{2,j} \approx (\psi_{5,j} - 6\psi_{4,j} + 18\psi_{3,j} - 10\psi_{2,j})/(-12h) \quad (21)$$

$$i = 3, 4, \dots, M + 1,$$

$$v_{i,j} \approx (\psi_{i+2,j} - 8\psi_{i+1,j} + 8\psi_{i-1,j} - \psi_{i-2,j})/12h \quad (22)$$

where

$$j = 2, 3, \dots, N$$

In computation, $i = 2, 3, \dots, M + 1$, $j = 2, 3, \dots, N$, in equations (15) and (16), and $i = 3, 4, \dots, M$, $j = 3, 4, \dots, N - 1$ in equation (17).

The boundary conditions (11), take the following finite-difference form:

(a) At the lower horizontal surface $0 \leq X \leq a/2$, $Y = 0$

$$w_{i,1} = \theta_{i,1} = \psi_{i,1} = 0$$

$$\psi_{i,2} \approx (3/4) \psi_{i,3} - (1/3) \psi_{i,4} + (1/16) \psi_{i,5} \quad (23)$$

where

$$i = 1, 2, \dots, M + 1$$

(b) At the upper horizontal surface $0 \leq X \leq a/2$, $Y = b$

$$w_{i,N+1} = \theta_{i,N+1} = \psi_{i,N+1} = 0$$

$$\psi_{i,N} \approx (3/4) \psi_{i,N-1} - (1/3) \psi_{i,N-2} + (1/16) \psi_{i,N-3} \quad (24)$$

where

$$i = 1, 2, \dots, M + 1$$

(c) At the vertical surface $X = 0$, $0 \leq Y \leq b$

$$w_{i,j} = \theta_{i,j} = \psi_{i,j} = 0$$

$$\psi_{2,j} \approx (3/4) \psi_{3,j} - (1/3) \psi_{4,j} + (1/16) \psi_{5,j} \quad (25)$$

where

$$j = 1, 2, \dots, N + 1$$

(d) At the vertical middle surface $X = a/2$, $0 < Y < b$

$$w_{M,j} = w_{M+2,j}, \theta_{M,j} = \theta_{M+2,j}, \psi_{M+1,j} = 0$$

$$\psi_{M,j} = -\psi_{M+2,j}, \quad \psi_{M-1,j} = -\psi_{M+3,j} \quad (26)$$

where

$$j = 2, 3, \dots, N$$

The finite-difference approximations for all the first order partial derivatives in this study are obtained by trying two, three, four and five grid points Taylor series expansion, and finally five grid point approximations were found to be reliable and satisfactory. The application of finite-difference method to free convection problems can be found in references [16 - 19].

3.2 Method of Solution

(a) Iterative Procedure

In this study, the successive-overrelaxation method discussed in reference [10] was employed to solve a set of finite-difference equations (15 - 22) and the associated boundary conditions (23 - 26). The procedure is discussed as follows.

1. The values of $w_{i,j}$ at each node point are obtained by solving equation (15) satisfying boundary condition and assuming $u_{i,j} = v_{i,j} = 0$ for all i 's and j 's.
2. The calculated values of $w_{i,j}$ and $u_{i,j} = v_{i,j} = 0$ are used in equation (16) to compute $\theta_{i,j}$ at all interior points and satisfy the corresponding boundary conditions.

It is noted that the above two steps correspond to the solution of uniformly heated (or cooled) laminar forced convection neglecting buoyancy effect due to the variation of temperature. The values of $w_{i,j}$ and $\theta_{i,j}$ are now used as the first approximations to the present secondary flow problem.

3. Substituting the calculated $\theta_{i,j}$ into equation (17) and keeping $u_{i,j} = v_{i,j} = 0$, the stream function $\psi_{i,j}$ at each node point can be found.
4. Using equations (18 - 22) the values for secondary flow $u_{i,j}$ and $v_{i,j}$ can be obtained for all the node points.
5. Using the values of $u_{i,j}$ and $v_{i,j}$ acquired in step 4, equations (15), (16) and (17) can be solved again for $w_{i,j}$, $\theta_{i,j}$ and $\psi_{i,j}$ respectively. The new values of $u_{i,j}$ and $v_{i,j}$ can be calculated from the latest $\psi_{i,j}$.
6. The above procedure is repeated until the maximum error is less than a prescribed small number ϵ .

The details of solving Poisson's equation and the inhomogeneous biharmonic equation by a point iterative method are to be discussed in APPENDIX B.

(b) Errors and Determination of Mesh Size

There are two important things in numerical calculation. One is the accuracy of the results and the other is the computing time. In the computation, errors can come from the following sources:

1. Round off error.

2. Finite-difference approximations for equations (15 - 26).
3. The convergence of each Poisson's and inhomogeneous biharmonic equation with the non-linear terms.

For error source 1, because of double precision (16 Figures) and a point iterative method used in this study, the round off errors should not be significant. For error source 2, this inherent error can be reduced by increasing the numbers of divisions M and N. A grid size test of the convergence of the numerical method was made. For each aspect ratio with $Ra C = 0$ and 10^6 , four or five sets of M and N (square network and even numbers; see APPENDIX B for details) were chosen. Some of the results are shown in Table 7 and Fig. 2. The number of divisions adopted are also listed in Table 7. For error source 3, the convergence of each Poisson's and inhomogeneous biharmonic equation including the non-linear terms is assured by continuing the computation until the following equation is satisfied.

$$|f_{i,j}^{(n+1)} - f_{i,j}^{(n)}|_{\max} / |f_{i,j}^{(n+1)}|_{\max} < \epsilon \quad (27)$$

where

$\epsilon = 5 \times 10^{-6}$ for each Poisson's and inhomogeneous biharmonic equation

$\epsilon = 1 \times 10^{-5}$ for secondary flow $u_{i,j}$ and $v_{i,j}$.

The convergence rate is faster for small numbers of divisions M

and N . In order to ascertain the convergence of finite-difference calculations, it is necessary to increase the values for M and N . But the larger the values of M and N , the slower the convergence rate, and the greater the computing time. For example in order to obtain a convergent solution satisfying condition (27) for $Ra_C = 0$ in a square channel ($\gamma = 1$) with $M = 16$ and $N = 32$, it is required to have 73 sweeps for the momentum equation and 56 sweeps for the energy equation. But if $M = 10$ and $N = 20$, it only takes 46 and 37 sweeps. The convergence of the solution for the inhomogeneous biharmonic equation is slow. Typically, it takes 3 to 5 minutes computing time for a complete solution for a number of values of parameter Ra_C for each aspect ratio by IBM 360 at the University of Alberta Computing Center.

The expressions $F(x,y)$ and $F'(x,y)$ in this chapter should be $F(x,y, \frac{\partial f}{\partial x}, \frac{\partial f}{\partial y})$ and $F'(x,y, \frac{\partial}{\partial x} \nabla^2 f, \frac{\partial}{\partial y} \nabla^2 f)$, respectively. These lead to non-symmetric matrices for linear algebraic equations.

CHAPTER IV

RESULTS AND DISCUSSION

4.1 Flow and Heat Transfer Characteristics

For the problem under consideration, velocity and temperature distributions, stream function, resistance coefficient and Nusselt number are usually of interest. Following the usual definitions the expressions for the product of friction factor and Reynolds number $f \cdot Re$ and the Nusselt number Nu can be written as follows:

$$f \cdot Re = \frac{\bar{\tau}_W}{\frac{1}{2} \rho \bar{W}^2} \cdot \frac{\bar{W} D_e \rho}{\mu} = \frac{2 \bar{\tau}_W D_e}{\mu \bar{W}} \quad (28)$$

$$Nu = \frac{\bar{h} D_e}{K} \quad (29)$$

where $\bar{\tau}_W$ and \bar{h} can be found directly by calculating the gradient of velocity and temperature on the boundary Γ respectively.

$$\bar{\tau}_W = \mu \left(\frac{\partial \bar{W}}{\partial n'} \right)_W \quad (30)$$

$$\bar{h} = \frac{-K \left| \frac{\partial \bar{T}}{\partial n'} \right|_W}{T_M}, \quad T_M = \frac{\int_A W(T - T_W) dA}{\int_A W dA} \quad (31)$$

Substituting equations (30) and (31) into (28) and (29), respectively, the following dimensionless forms can be obtained.

$$f \cdot Re = \frac{2 \left(\frac{\partial \bar{w}}{\partial n} \right)_W}{\bar{w}} \quad (32)$$

$$Nu = \frac{\left| \frac{\partial \bar{\theta}}{\partial n} \right|_W \bar{w}}{|\bar{w}\bar{\theta}|_W} \quad (33)$$

Also $\bar{\tau}_W$ and \bar{h} can be obtained by considering overall force and energy balances, respectively.

$$\bar{\tau}_W = \frac{dP_0}{dZ} \cdot \frac{A}{S} = c_1 \frac{A}{S} = c_1 \frac{D_e}{4} \quad (34)$$

$$\bar{h} = \rho c_p \frac{\partial T}{\partial Z} \cdot \frac{\bar{W} \cdot A}{T_M \cdot S} = \frac{\rho c_p c_2 \bar{W} \cdot D_e}{4 T_M} \quad (35)$$

The results are

$$f \cdot Re = 2/\bar{w} \quad (36)$$

$$Nu = \bar{w}^2/4 |\bar{w}\bar{\theta}| \quad (37)$$

Equations (32), (33), (36), and (37) imply that

$$\left(\frac{\partial \bar{w}}{\partial n} \right)_W = 1 \text{ and } \left| \frac{\partial \bar{\theta}}{\partial n} \right|_W = \bar{w}/4 \quad (38)$$

Some of these numerical values are listed in Table 8. It can be seen that the difference between these two methods is around 0.3% for all the cases considered. The values given in Tables 1 - 6 are computed by using equation (32) and (33). The above average quantities such as \bar{w} , $\frac{\partial \bar{w}}{\partial n}$, $\bar{w\theta}$ and $\frac{\partial \bar{\theta}}{\partial n}$ are obtained by using Simpson's rule.

4.2 ReRa Number Effects

To illustrate the effect of the product of Reynolds and Rayleigh number on the axial velocity and temperature distributions, the profiles along the vertical axis $X = a/2$ are plotted for the aspect ratio $\gamma = 1$, $Pr = 0.73$ in Figs. 3 and 4. It is seen clearly that the effect of the secondary flow is to shift the location of the maximum value downward and decrease the magnitude of the maximum value as the parameter ReRa increases. The velocity and temperature distributions along the horizontal axis $Y = b/2$ for $\gamma = 1$, $Pr = 0.73$ with ReRa as a parameter are shown in Fig. 5. As expected, the magnitude of these profiles decreases as ReRa increases. In Fig. 6, streamlines and isotherms are plotted for a square channel $\gamma = 1$ with $Pr = 0.73$ and $ReRa = 1.030 \times 10^5$. It is interesting to observe that, due to the higher density at the center of vortex, the location of the maximum value of stream function ψ or the center of circulation is lower than the horizontal central axis, $Y = b/2$. One also notes that the value of stream function at a given point is proportional to the flow rate crossing any path joining the point and the wall. Although not shown here, the value

of the stream function or the intensity of secondary flow increases as the value of the parameter $ReRa$ increases. The effect of buoyancy force on temperature distribution is also clearly seen in the distributions of the isotherms on the right hand side of this figure.

4.3 Aspect Ratio Effects

In order to see the effect of aspect ratio on flow and heat transfer characteristics, the rectangular channels with long side horizontal will be considered first. The velocity and temperature distributions along the vertical axis $X = a/2$ are plotted for the aspect ratio $\gamma = 2$ and $Pr = 0.73$ with $ReRa$ as a parameter in Figs. 7 and 8. The velocity and temperature profiles along the horizontal axis $Y = b/2$ for $\gamma = 2$ and $Pr = 0.73$ are shown in Fig. 9. Nearly the same trend exists for $\gamma = 2$ as for $\gamma = 1$. Streamlines and isotherms for $\gamma = 2$, $Pr = 0.73$ and $ReRa = 1.408 \times 10^5$ are presented in Fig. 10. For this case, the center of circulation is seen to be located almost along the horizontal central axis $Y = b/2$. However, the location of minimum temperature (for heating or positive $ReRa$) is still found below the horizontal axis $Y = b/2$. The pattern of the streamline shows that the intensity of the secondary flow near the vertical wall is stronger than the central core region.

The effect of aspect ratio can further be seen for $\gamma = 5$. The velocity and temperature profiles along the vertical central axis $X = a/2$ are plotted in Figs. 11 and 12, respectively, with $Pr = 0.73$ and $ReRa = 0$ and 2.984×10^5 . The velocity and temperature profiles along the hori-

zontal central axis $Y = b/2$ are shown in Fig. 13. These figures show that the secondary flow has less effect on the velocity and temperature distributions in the central region for higher aspect ratio γ . This phenomenon can be seen also from Fig. 14 where the streamlines and isotherms are shown for $\gamma = 5$. It is seen that the secondary flow is weak in the central region and rather intense near the short vertical wall. The center of circulation for this case is almost along the central horizontal axis $Y = b/2$. The streamlines for the rectangular channels with $\gamma = 1, 2$ and 5 show clearly that as the aspect ratio γ increases, the location of the center of circulation tends to move toward the vertical short wall. As a result of this, the secondary flow is rather weak in central region and intense near the vertical wall. It is noted that for $\gamma = 2$ and 5 , the center of circulation is almost along the horizontal central axis whereas for $\gamma = 1$, the center of circulation is well below the central horizontal axis for $ReRa = 1.030 \times 10^5$.

The effect of aspect ratio when the long side is vertical will be considered next. The velocity and temperature distributions along central axes $X = a/2$ and $Y = b/2$ are shown in Figs. 15, 16 and 17 for a rectangular channel with aspect ratio $\gamma = 0.5$, $Pr = 0.73$ with $ReRa$ as a parameter. Comparing with the case $\gamma = 2$, one notes that in general the location of the maximum value for velocity and temperature profiles moves closer to the bottom horizontal wall. The streamline and isotherms for the aspect ratio $\gamma = 0.5$, $Pr = 0.73$ and $ReRa = 1.381 \times 10^5$ are shown in Fig. 18. One sees that the center of circulation is well below the hori-

zontal central axis and the secondary flow motion is weak in the upper region and rather intense near the bottom horizontal wall. Because of rather intense secondary motion, large temperature gradients exist near the bottom horizontal wall.

The graphical results for velocity and temperature distributions for $\gamma = 0.2$, $Pr = 0.73$, $ReRa = 0, 2.535 \times 10^5$ are shown in Figs. 19, 20 and 21. For this case the location of the maximum magnitude for both velocity and temperature is seen to be quite close to the bottom horizontal wall. The streamlines and isotherms for $\gamma = 0.2$, $Pr = 0.73$ and $ReRa = 2.535 \times 10^5$ are shown in Fig. 22. Once again one sees that stronger secondary motion exists near the narrow bottom horizontal wall. Correspondingly, larger temperature gradients exist there. Comparing with the case $\gamma = 0.5$, one notes that the center of circulation and location of the minimum magnitude of temperature move further downward.

4.4 Results of \bar{w}/\bar{w}_0 , $fRe/(fRe)_0$, Nu/Nu_0 and Pr Number Effect

It may be of some interest to compare the relations between \bar{w}/\bar{w}_0 and $ReRa$ for various aspect ratios considered. The results are shown in Fig. 23 for $Pr = 0.73$. The effect of secondary flow on the average axial velocity is greatest for $\gamma = 1$ and decrease as $\gamma \rightarrow 0$ or ∞ . A plot of the ratio of the product of friction factor and Reynolds number with and without buoyancy effect $fRe/(fRe)_0$ versus the parameter $ReRa$ is presented in Fig. 24 for $Pr = 0.73$ with aspect ratio γ as a parameter. A similar plot for the ratio of Nusselt number with and without buoyancy

effect Nu/Nu_0 is shown in Fig. 25. In order to see the effect of Prandtl number on heat transfer, the result for $\gamma = 1$, and $Pr = 7.2$ is also shown in the same figure. Since the effects of Prandtl number on the ratios \bar{w}/\bar{w}_0 and $fRe/(fRe)_0$ are not very significant, the results for the case $Pr = 7.2$ are not shown in Fig. 23 and 24 (see Table 2 and equations (8 - 10) also).

4.5 Conclusions

1. The method of successive-overrelaxation can be applied to combined free and forced laminar convection in long horizontal rectangular channels with various aspect ratios. Unfortunately, this method diverges for the values of the parameter $ReRa$ beyond those shown in Figs. 23 - 25 and Tables 1 - 6. The exact reasons for the divergence of the solution were unknown to the author. However, it was found that the numerical values of the terms $\nabla^2 \nabla^2 \psi$, $\nabla^2 w$ and $\nabla^2 \theta$ approach zero as the values of $ReRa$ becomes larger than indicated. This effect can also be seen in normalization analysis (see APPENDIX A). These terms are all of the order of $1/Gr^{1/2}$. Despite this difficulty, the method yields a satisfactory solution for a range of $ReRa$ far exceeding that of Morton's perturbation method [1] for laminar convection in uniformly heated horizontal pipes in error by about 10% for $RaC = 3.84 \times 10^5$.

2. As can be expected, the resistance coefficient and the Nusselt number increase as the value of $ReRa$, representing buoyancy effect, increases. The effect of aspect ratio on flow and heat transfer characteristics is clearly seen in Figs. 24 and 25. For the aspect ratio $\gamma = 1$, the effect of Prandtl number is considerable. As similar effect can be expected for other aspect ratios.
3. The details of secondary motion caused by buoyancy forces are clearly seen from the pattern of streamlines from which it is evident that there are two vortices with opposite sense formed. It is also noted that for a square channel the center of circulation is well below the central horizontal axis. One can visualize the secondary flow motion by noting that the flow rate through any line connecting the center of circulation and a point on the wall is constant for a given value of the parameter $ReRa$. For a rectangular channel, with long side horizontal, as the aspect ratio γ increases, the intensity of secondary motion near the short vertical wall increases. For a rectangular channel with long side vertical, as the aspect ratio decreases, the center of circulation moves toward the bottom short horizontal wall. Consequently, intense secondary motion exists near the bottom wall.
4. The method used here has also been applied to a circular pipe as Morton did in [1]. But due to the slow convergence of the

inhomogeneous biharmonic equation in polar coordinates and the difficulty with boundary conditions for the vorticity function, it did not work well.

5. The perturbation method used by Morton may be applied here if numerical integration is used instead of an analytical method of solution. This possibility is discussed in APPENDIX C.

REFERENCES

1. B.R. Morton, "Laminar Convection in Uniformly Heated Horizontal Pipes at Low Rayleigh Numbers", Quarterly Journal of Mechanics and Applied Mathematics, Vol. 12, Pt. 4, 1959, pp. 410-420.
2. E. del Casal and W.N. Gill, "A Note on Natural Convection Effects in Fully Developed Horizontal Tube Flow", A.I.Ch.E. Journal, Vol. 8, No. 4, 1962, pp. 570-574.
3. W.N. Gill and E. del Casal, "A Theoretical Investigation of Natural Convection Effects in Forced Horizontal Flows", A.I.Ch.E. Journal, Vol. 8, No. 4, 1962, pp. 513-518.
4. Y. Mori and K. Futagami, "Forced Convective Heat Transfer in Horizontal Tubes (2nd Report, Theoretical Study on the Effect of Buoyancy)", Trans. of the Japan Society of Mechanical Engineers, Vol. 32, No. 233, 1966, pp. 88-97.
5. Y. Mori, K. Futagami, S. Tokuda and M. Nakamura, "Forced Convective Heat Transfer in Uniformly Heated Horizontal Tubes, 1st report - Experimental Study on the Effect of Buoyancy", International Journal of Heat and Mass Transfer, Vol. 9, No. 5, 1966, pp. 453-463.
6. M. Iqbal and J.W. Stachiewicz, "Influence of Tube Orientation on Combined Free and Forced Laminar Convection Heat Transfer", Journal of Heat Transfer, Trans. ASME, Series C, Vol. 88, No. 1, 1966, pp. 109-116.

7. S.T. McComas and E.R.G. Eckert, "Combined Free and Forced Convection in a Horizontal Circular Tube", Journal of Heat Transfer, Trans. ASME, Series C, Vol. 88, No. 2, 1966, pp. 147-153.
8. L.S. Han, "Laminar Heat Transfer in Rectangular Channels", Journal of Heat Transfer, Trans. ASME, Series C, Vol. 81, 1959, pp. 121-128.
9. L.N. Tao, "On Combined Free and Forced Convection in Channels", Journal of Heat Transfer, Trans. ASME, Series C, Vol. 82, 1960, pp. 233-238.
10. D. Young, "The Numerical Solution of Elliptic and Parabolic Partial Differential Equation", in Survey of Numerical Analysis, J. Todd, editor, McGraw-Hill Book Company, Inc., New York, N.Y. 1962.
11. W.D. Morris, "Laminar Convection in a Heated Vertical Tube Rotating About a Parallel Axis", Journal of Fluid Mechanics, Vol. 21, Pt. 3, 1965, pp. 453-464.
12. Y. Mori and W. Nakayama, "Forced Convective Heat Transfer in a Straight Pipe Rotating Around a Parallel Axis (1st Report, Laminar Region)", International Journal of Heat and Mass Transfer, Vol. 10, No. 9, 1967, pp. 1179-1194.
13. Y. Mori and W. Nakayama, "Study on Forced Convective Heat Transfer in Curved Pipes (1st Report, Laminar Region)", International Journal of Heat and Mass Transfer, Vol. 8, No. 1, 1965, pp. 67-82.

14. Y. Mori and Y. Uchida, "Forced Convective Heat Transfer in a Curved Channel", JSME 1967 Semi-International Symposium, Heat and Mass Transfer, Thermal Stress Vol. 1, pp. 181-190.
15. Y. Mori, W. Nakayama and Y. Uchida, "Convective Heat Transfer in Ducts with Secondary Flow", Journal of the Japan Society of Mechanical Engineers, Vol. 70, No. 583, 1967, pp. 1188-1196.
16. S.W. Churchill, "The Prediction of Natural Convection", Proceedings of the Third International Heat Transfer Conference, A.I.Ch.E., Vol. 6, 1966, pp. 15-30.
17. J.O. Wilkes and S.W. Churchill, "The Finite-Difference Computation of Natural Convection in a Rectangular Enclosure", A.I.Ch.E. Journal Vol. 12, No. 1, 1966, pp. 161-166.
18. M.R. Samuels and S.W. Churchill, "Stability of a Fluid in a Rectangular Region Heated from Below", A.I.Ch.E. Journal, Vol. 13, No. 1, 1967, pp. 77-85.
19. H.Z. Barakat and J.A. Clark, "Analytical and Experimental Study on the Transient Laminar Natural Convection Flows in Partially Filled Liquid Containers", Proceedings of the Third International Heat Transfer Conference, A.I.Ch.E., Vol. 2, 1966, pp. 152-162.
20. S.M. Marco and L.S. Han, "A Note on Limiting Laminar Nusselt Number in Ducts with Constant Temperature Gradient by Analogy to Thin-Plate Theory", Trans. ASME, Vol. 77, 1955, pp. 625-630.

APPENDIX A

NORMALIZATION OF EQUATIONS

To normalize the governing equations, first introduce the following dimensionless quantities,

$$X = D_e x, Y = D_e y, Z = Lz, U = V_c u, V = V_c v$$

$$W = \bar{W} W, P_0 = P_c p_0, T - T_W = C_2 D_e \theta \quad (A.1)$$

The pressure terms can be eliminated between the momentum equations in X and Y directions. Noting that the driving forces (axial pressure gradient and buoyancy forces) and the inertia terms can be considered as the same order of magnitude and defining characteristic quantities,

$$V_c = (\beta g C_2 D_e)^{1/2} = Gr^{1/2} \nu / D_e,$$

$$P_c = \nu \rho \bar{W} Gr^{1/2} L / D_e = \rho \bar{W}^2 (Gr^{1/2} / Re)(L / D_e) \quad (A.2)$$

then the governing equations can be written as follows,

$$\partial u / \partial x + \partial v / \partial y + \epsilon_1 \partial w / \partial z = 0$$

$$\xi = \partial u / \partial y - \partial v / \partial x$$

$$u \partial \xi / \partial x + v \partial \xi / \partial y + \epsilon_1 w \partial \xi / \partial z = \nabla^2 \xi / Gr^{1/2} + \epsilon_2 \partial^2 \xi / \partial z^2 - \partial \theta / \partial x$$

$$u \partial w / \partial x + v \partial w / \partial y + \epsilon_1 w \partial w / \partial z = - \partial P_0 / \partial z + \nabla^2 w / Gr^{1/2} + \epsilon_2 \partial^2 w / \partial z^2$$

$$u \partial \theta / \partial x + v \partial \theta / \partial y + \epsilon_1 w \partial \theta / \partial z = \nabla^2 \theta / (Pr Gr^{1/2}) + \epsilon_2 \partial^2 \theta / \partial z^2 + \Phi$$

$$\Phi = \epsilon_3 [2\{(\partial u / \partial x)^2 + (\partial v / \partial y)^2\} + (\partial v / \partial x + \partial u / \partial y)^2$$

$$+ (D_e / L)^2 \{(\partial v / \partial z)^2 + (\partial u / \partial z)^2\}]$$

$$+ \epsilon_4 [2(D_e / L)^2 (\partial w / \partial z)^2 + (\partial w / \partial y)^2 + (\partial w / \partial x)^2]$$

$$+ \epsilon_5 [2(D_e / L)^2 \{(\partial w / \partial y) (\partial v / \partial z) + (\partial u / \partial z) (\partial w / \partial x)\}] \quad (A.3)$$

where

$$\epsilon_1 = (Re / Gr^{1/2}) (D_e / L) , \quad \epsilon_2 = (D_e / L)^2 / Gr^{1/2}$$

$$\epsilon_3 = Os / Gr^{1/2} , \quad \epsilon_4 = Ec / Gr^{1/2} , \quad \epsilon_5 = Ec / Re \quad (A.4)$$

Since the flow is fully developed, $D_e/L \ll 1$ and viscous dissipations are negligible i.e. $0s \ll 1$ and $Ec \ll 1$. Thus, all the terms with coefficients ϵ_i ($i = 1, 2, \dots, 5$) can be neglected, and the above equations (A.3) can be written as,

$$\partial u / \partial x + \partial v / \partial y = 0$$

$$\xi = \partial u / \partial y - \partial v / \partial x$$

$$u \partial \xi / \partial x + v \partial \xi / \partial y = \nabla^2 \xi / Gr^{1/2} - \partial \theta / \partial x$$

$$u \partial w / \partial x + v \partial w / \partial y = - \partial P_0 / \partial z + \nabla^2 w / Gr^{1/2}$$

$$u \partial \theta / \partial x + v \partial \theta / \partial y = \nabla^2 \theta / (Pr Gr^{1/2}) \quad (A.5)$$

It is noted that if the value of Gr number is less than the order of 10^3 , then the terms $\nabla^2 \xi / Gr^{1/2}$, $\nabla^2 w / Gr^{1/2}$ and $\nabla^2 \theta / (Pr Gr^{1/2})$ can not be neglected. In contrast, Mori et al [4] neglected these terms in their analysis for higher value of Gr number.

APPENDIX B

METHOD OF SOLVING EQUATIONS $\nabla^2 f = F$ AND $\nabla^4 f = F'$

It is desirable to discuss a procedure for solving the Poisson's equation $\nabla^2 f = F(x,y)$ and inhomogeneous biharmonic equation $\nabla^4 f = F'(x,y)$ with the associated boundary conditions by a point iterative method which was mentioned in 3.2. The finite-difference approximation of Poisson's equation (13) can be rewritten as

$$f_{i,j} \approx A_1(f_{i+1,j} + f_{i-1,j}) + A_2(f_{i,j+1} + f_{i,j-1}) - A_3 F_{i,j} \quad (B.1)$$

where

$$A_1 = \frac{\ell^2}{2(h^2 + \ell^2)}, \quad A_2 = \frac{h^2}{2(h^2 + \ell^2)}, \quad A_3 = \frac{h^2 \ell^2}{2(h^2 + \ell^2)}$$

At the beginning, prescribe the value of boundary points and let $f_{i,j} = 0$ for all i 's and j 's in the region. The calculation is executed from $i = 2$, $j = 2$ along the column $i = 2$. For example, the value of $f_{2,2}$ is computed by

$$f_{2,2} = A_1 (0 + f_{1,2}) + A_2 (0 + f_{2,1}) - A_3 F_{2,2} \quad (B.2)$$

The newly obtained value $f_{2,2}$ is used in the computation of $f_{2,3}$ by

$$f_{2,3} = A_1(0 + f_{1,3}) + A_2(0 + f_{2,2}) - A_3 F_{2,3} \quad (B.3)$$

This process is continued up to $j = N$ and then similar process is reported for a new column $i = 3$ and the succeeding columns until the last column $i = M + 1$ is reached. After completing one whole sweep, the calculation is back to $i = 2, j = 2$ again. For example,

$$f_{2,2} = A_1(f_{3,2} + f_{1,2}) + A_2(f_{2,3} + f_{2,1}) - A_3 F_{2,2} \quad (B.4)$$

where the values of $f_{3,2}$ and $f_{2,3}$ come from the results of the first sweep. The above process is repeated until equation (27) is satisfied. Then a numerical solution $f_{i,j}$ which satisfy the Poisson's equation and the associated boundary condition is obtained.

The method of solution for $\nabla^4 f = F'(x,y)$ is similar to the above except that the computation is started from $i = 3, j = 3$ and the values of boundary and adjacent points are obtained by two boundary conditions.

In carrying out the above calculations, the following formula for successive-overrelaxation is used [10]:

$$\begin{aligned} f_{i,j}^{(n+1)} = & \omega[A_1(f_{i+1,j}^{(n)} + f_{i-1,j}^{(n+1)}) + A_2(f_{i,j+1}^{(n)} + f_{i,j-1}^{(n+1)}) \\ & - A_3 F_{i,j}] - (\omega - 1) f_{i,j}^{(n)} \end{aligned} \quad (B.5)$$

The superscript (n) denotes that the values obtained by the previous sweep. The relaxation factor ω is calculated by the following equation [10],

$$\omega = 1 + [\bar{\mu}/\{1 + (1 - \bar{\mu}^2)^{1/2}\}]^2 \quad (\text{B.6})$$

where

$$\bar{\mu} = \left(\frac{1}{2}\right) \left(\cos \frac{\pi h}{a} + \cos \frac{\pi h}{b}\right), \quad (\text{B.7})$$

$a/2 = Mh$, $b = Nh$ and $h = \text{mesh size}$.

It is noted that the square network $h = \ell$ was used for all the cases considered in this study and even numbers of M and N were taken for the purpose of applying Simpson's numerical integration. The values for the relaxation factor ω calculated by equation (B.6) are optimum only for essentially self-adjoint equations.

APPENDIX C

PERTURBATION METHOD

Solution of equation (8 - 10) and boundary condition (11) can also be obtained by expanding ψ , w , and θ as power series in the product of Rayleigh number and C , provided that this is numerically small.

$$\psi = (RaC) \psi_1 + (RaC)^2 \psi_2 + \dots$$

$$w = w_0 + (RaC)w_1 + (RaC)^2 w_2 + \dots$$

$$\theta = \theta_0 + (RaC)\theta_1 + (RaC)^2 \theta_2 + \dots \quad (C.1)$$

The leading term ψ_0 of ψ must vanish because there is no circulation when buoyancy effect is neglected or $RaC = 0$. After substituting the above power series into equation (8 - 10), ψ_i , w_i and θ_i are obtained by equating coefficients of the same powers of RaC . The coefficients of $(RaC)^0$ are

$$\nabla^2 w_0 + 4 = 0$$

$$\nabla^2 \theta_0 + w_0 = 0 \quad (C.2)$$

The coefficients of (RaC) are

$$\nabla^4 \psi_1 - \frac{\partial \theta_0}{\partial x} = 0$$

$$\frac{\partial \psi_1}{\partial y} \frac{\partial w_0}{\partial x} - \frac{\partial \psi_1}{\partial x} \frac{\partial w_0}{\partial y} = \nabla^2 w_1$$

$$\text{Pr} \left(\frac{\partial \psi_1}{\partial y} \frac{\partial \theta_0}{\partial x} - \frac{\partial \psi_1}{\partial x} \frac{\partial \theta_0}{\partial y} \right) = \nabla^2 \theta_1 - w_1 \quad (\text{C.3})$$

and so on.

It is quite tedious to obtain an analytic solution of the above equations in a rectangular channel. Thus any numerical methods can be used to solve them. Due to the existence of errors in numerical solutions of (C.2), (C.3),--and, recalling the product of $(\text{RaC})^n$ and ψ_n (or w_n , θ_n) in Series (C.1), the error of the solution ψ (or w , θ) become uncontrollable when the value of RaC becomes larger. The rather limited ranges of RaC and the unknown errors are the reasons that this method were not tried here.

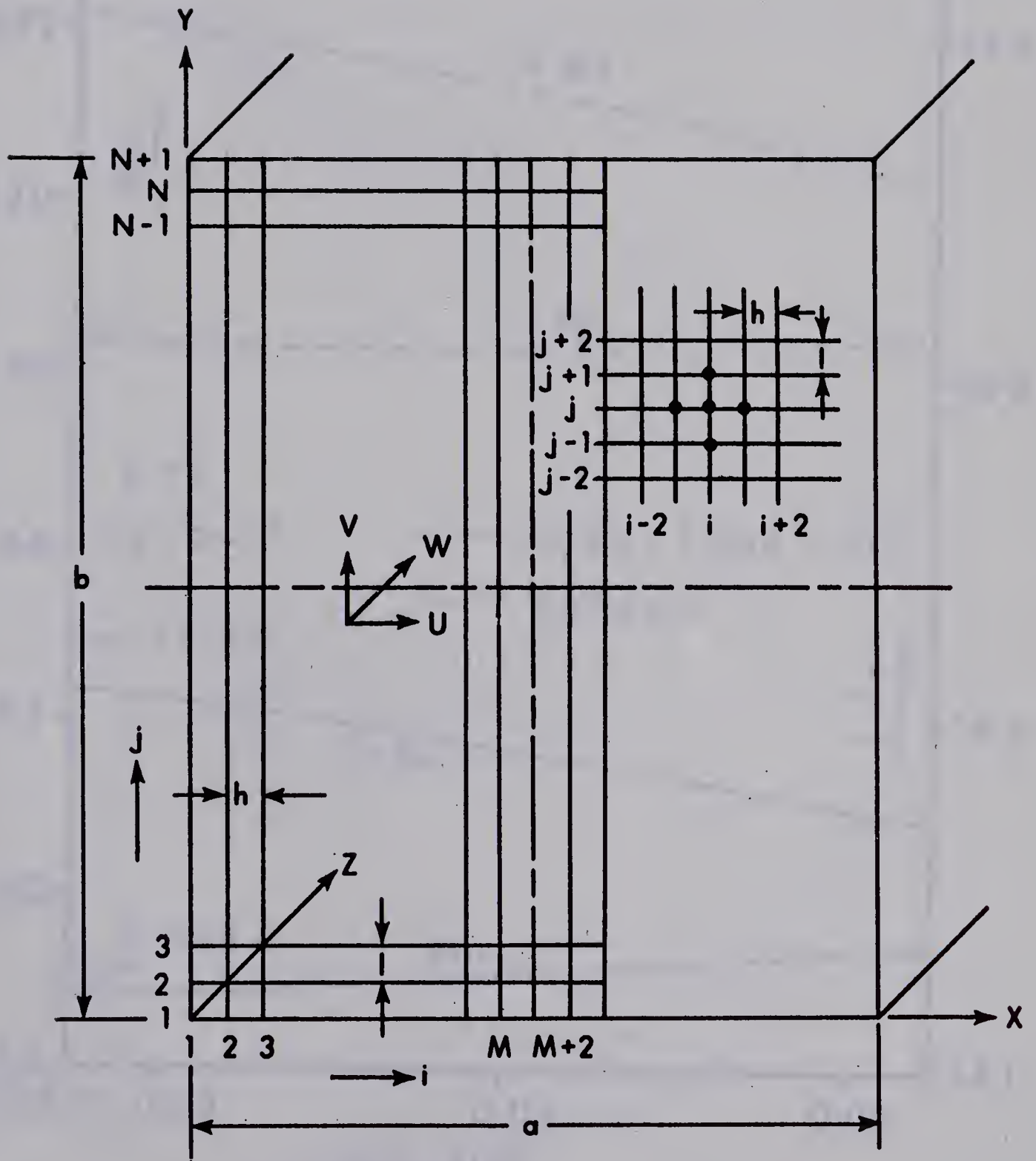


Fig. 1 Coordinate System and Finite Difference Network For A Rectangular Channel

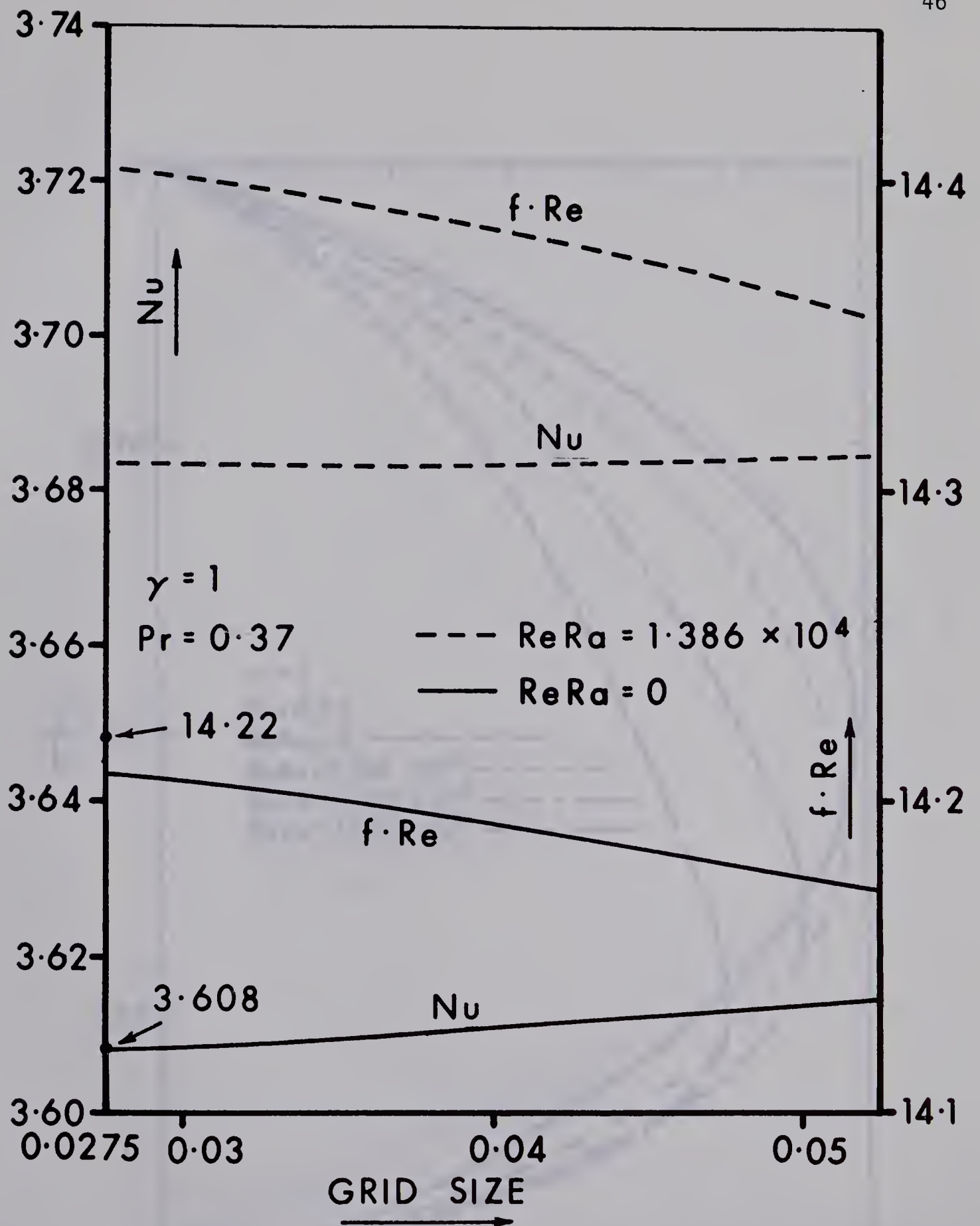


Fig. 2 Effect of Grid Size on Flow and Heat Transfer Results for Square Channel $\gamma = 1$, With $Pr = 0.73$ and $ReRa = 0$ and 1.386×10^4

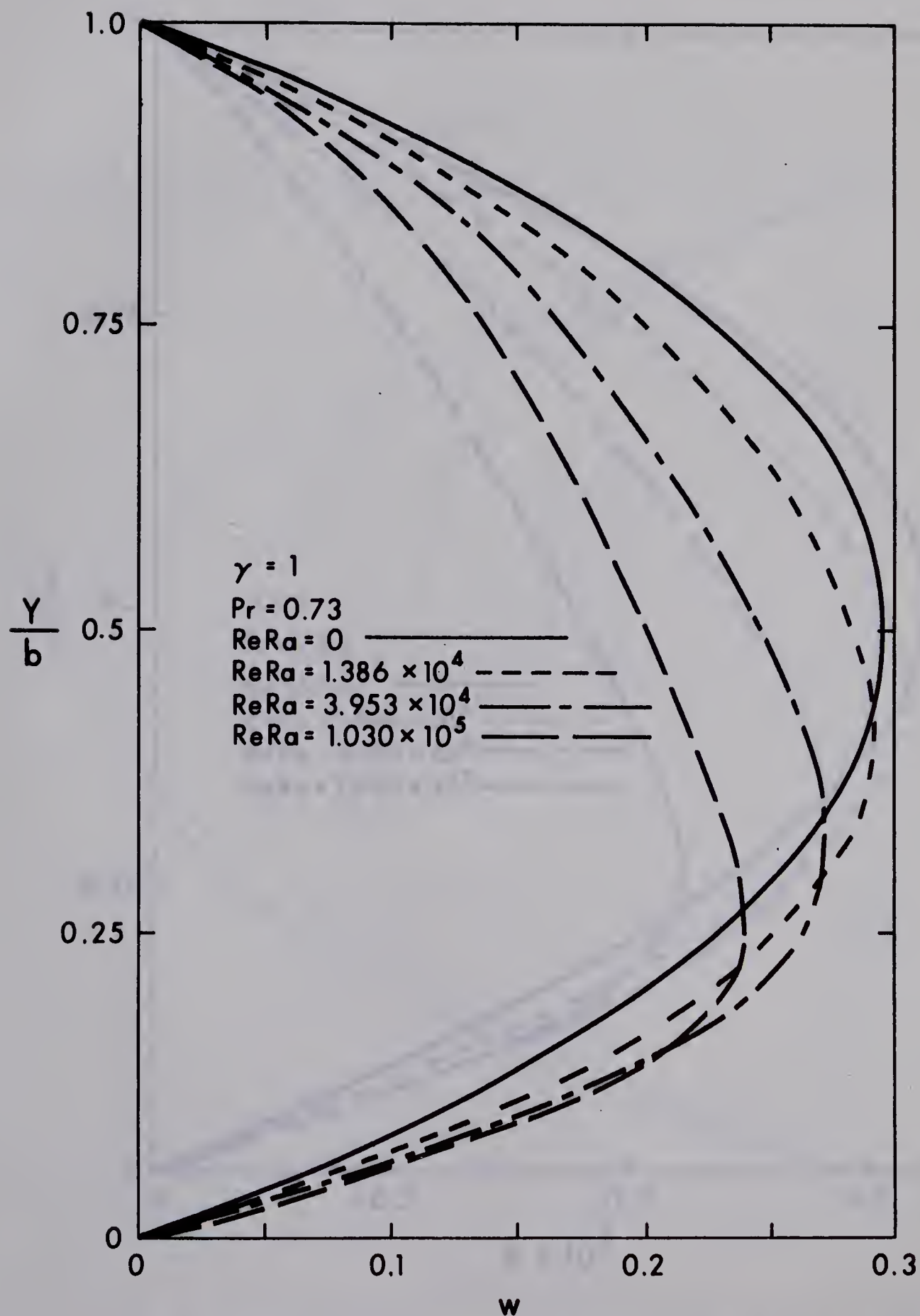


Fig. 3 Dimensionless Axial Velocity Distribution at $X = a/2$ With $ReRa$ as a Parameter in a Square Channel $\gamma = 1$ and $Pr = 0.73$

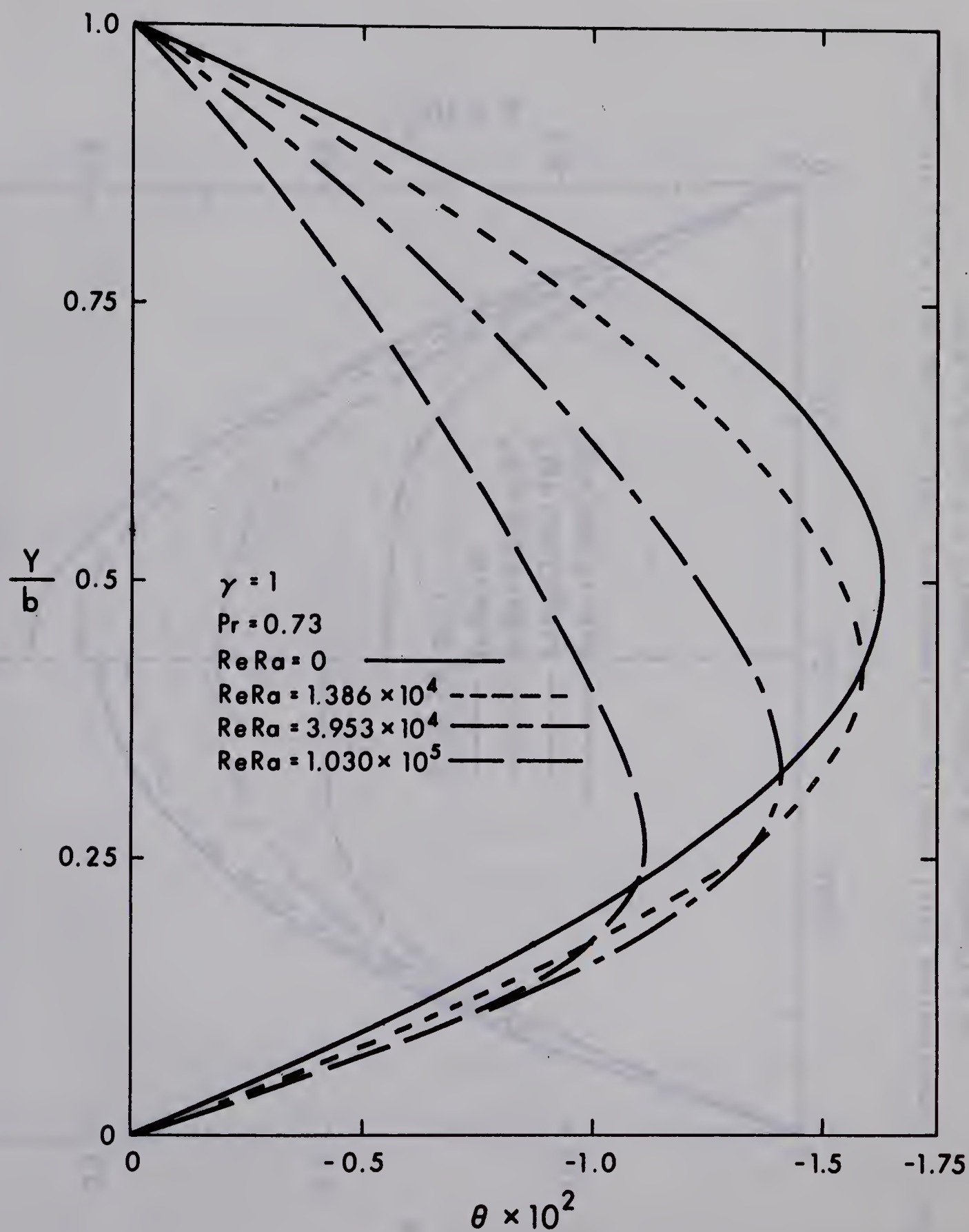


Fig. 4 Dimensionless Temperature Distribution at $X = a/2$ With $ReRa$ as a Parameter in a Square Channel $\gamma = 1$ and $Pr = 0.73$

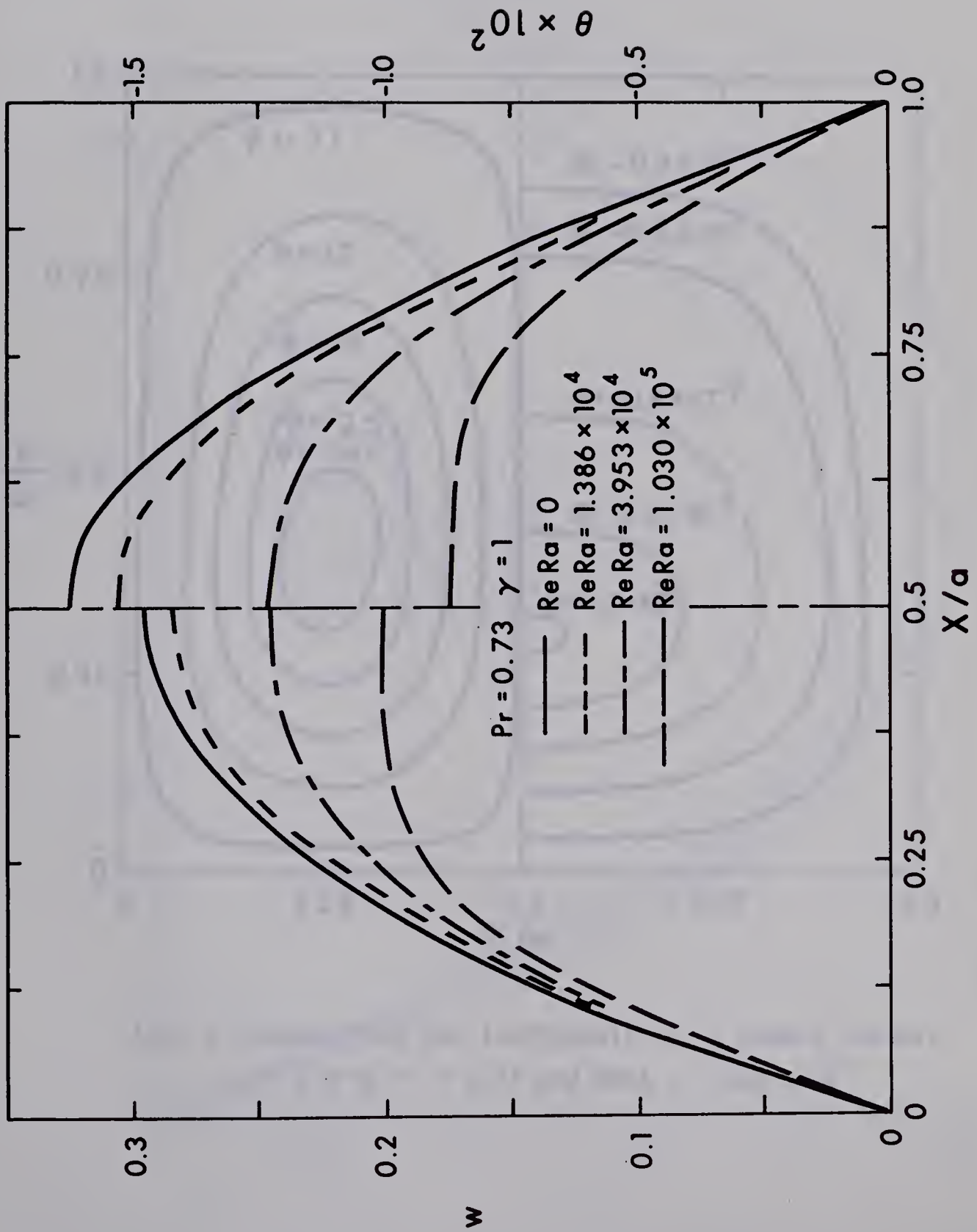


Fig. 5 Dimensionless Axial Velocity and Temperature Distributions at $Y = b/2$ With $ReRa$ as a Parameter in a Square Channel $\gamma = 1$ and $Pr = 0.73$

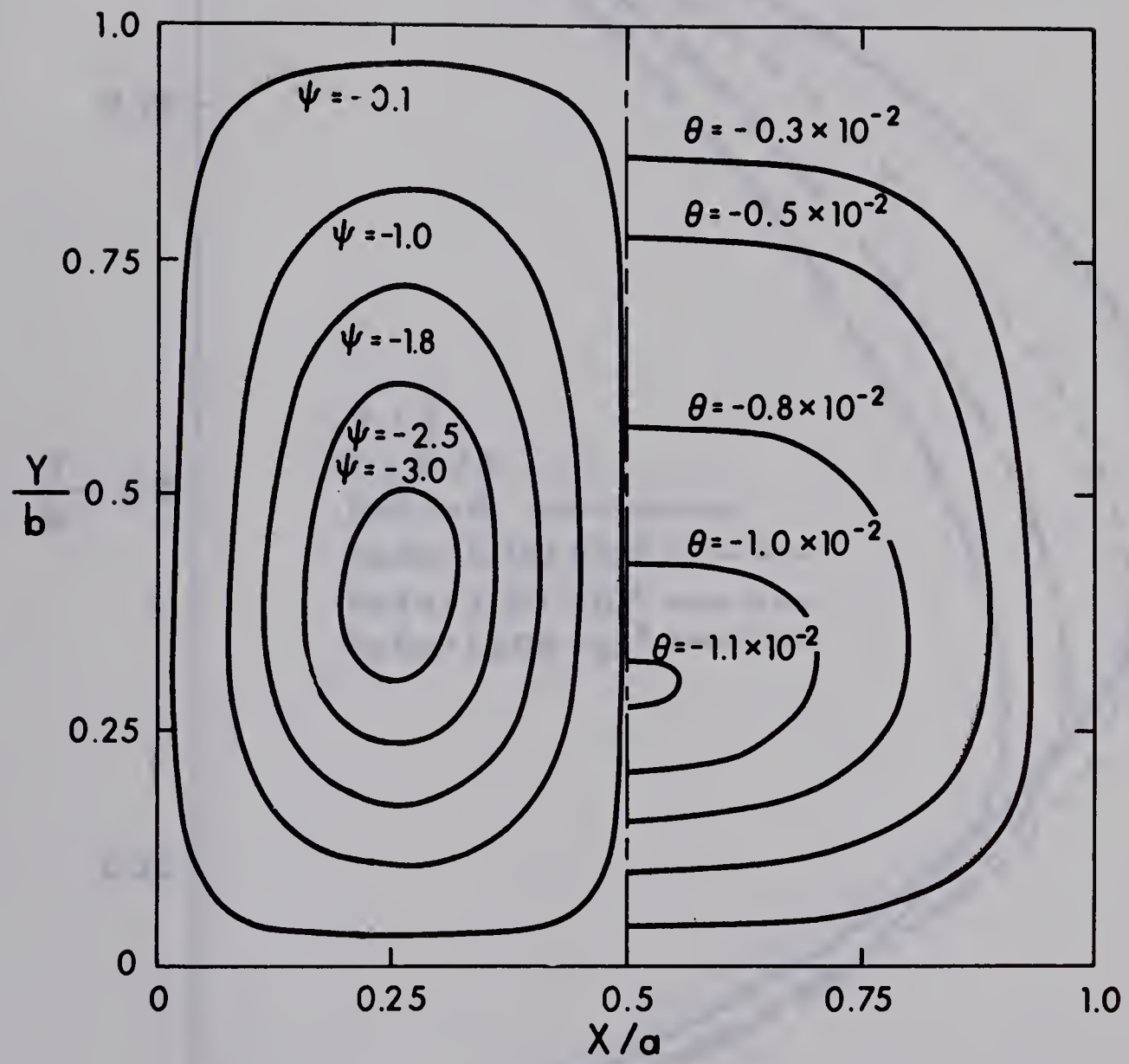


Fig. 6 Streamlines and Isotherms for a Square Channel.
 $\gamma = 1$ With $Pr = 0.73$ and $ReRa = 1.030 \times 10^5$

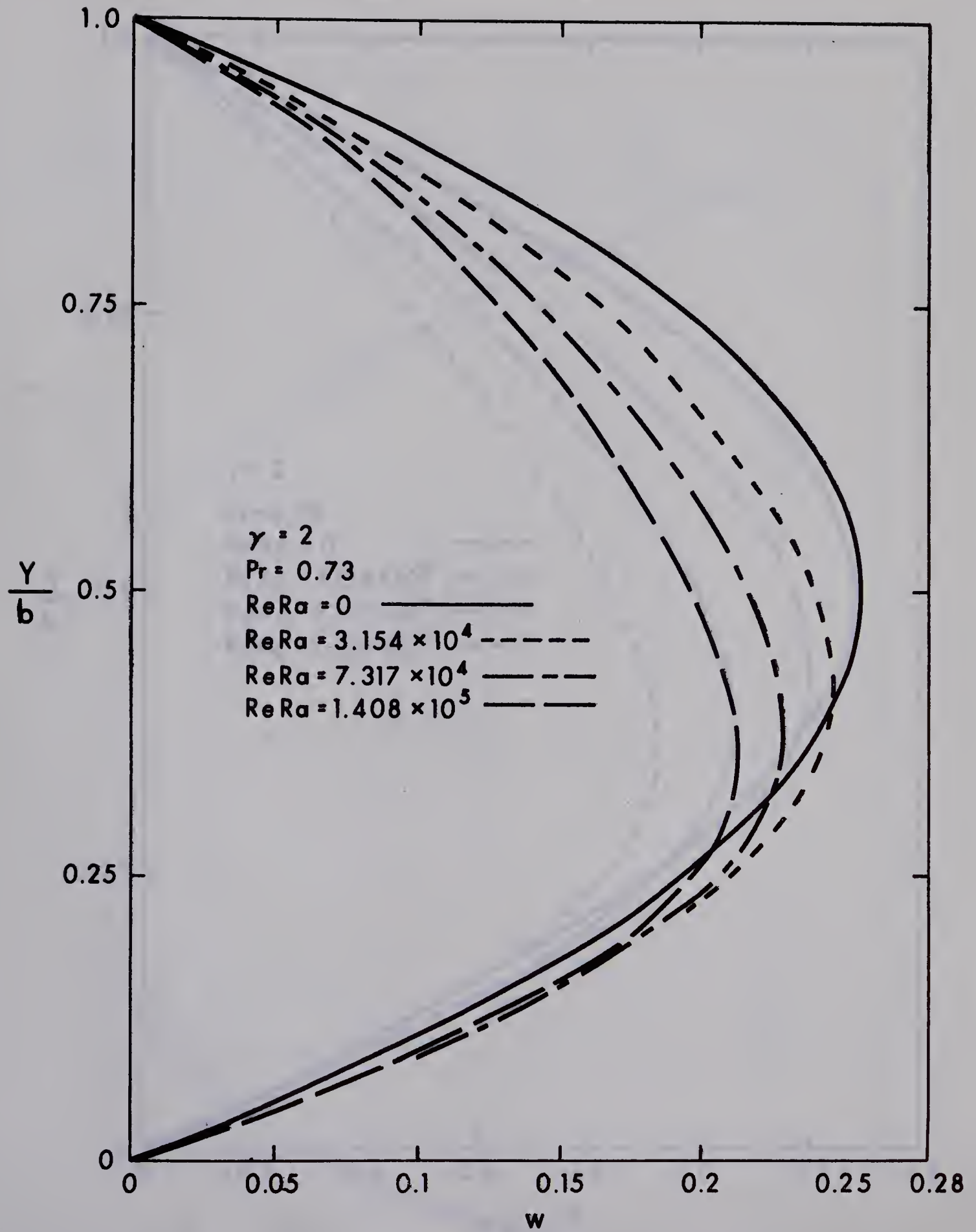


Fig. 7 Dimensionless Axial Velocity Distribution at $X = a/2$ With $ReRa$ as a Parameter in a Rectangular Channel $\gamma = 2$ and $Pr = 0.73$

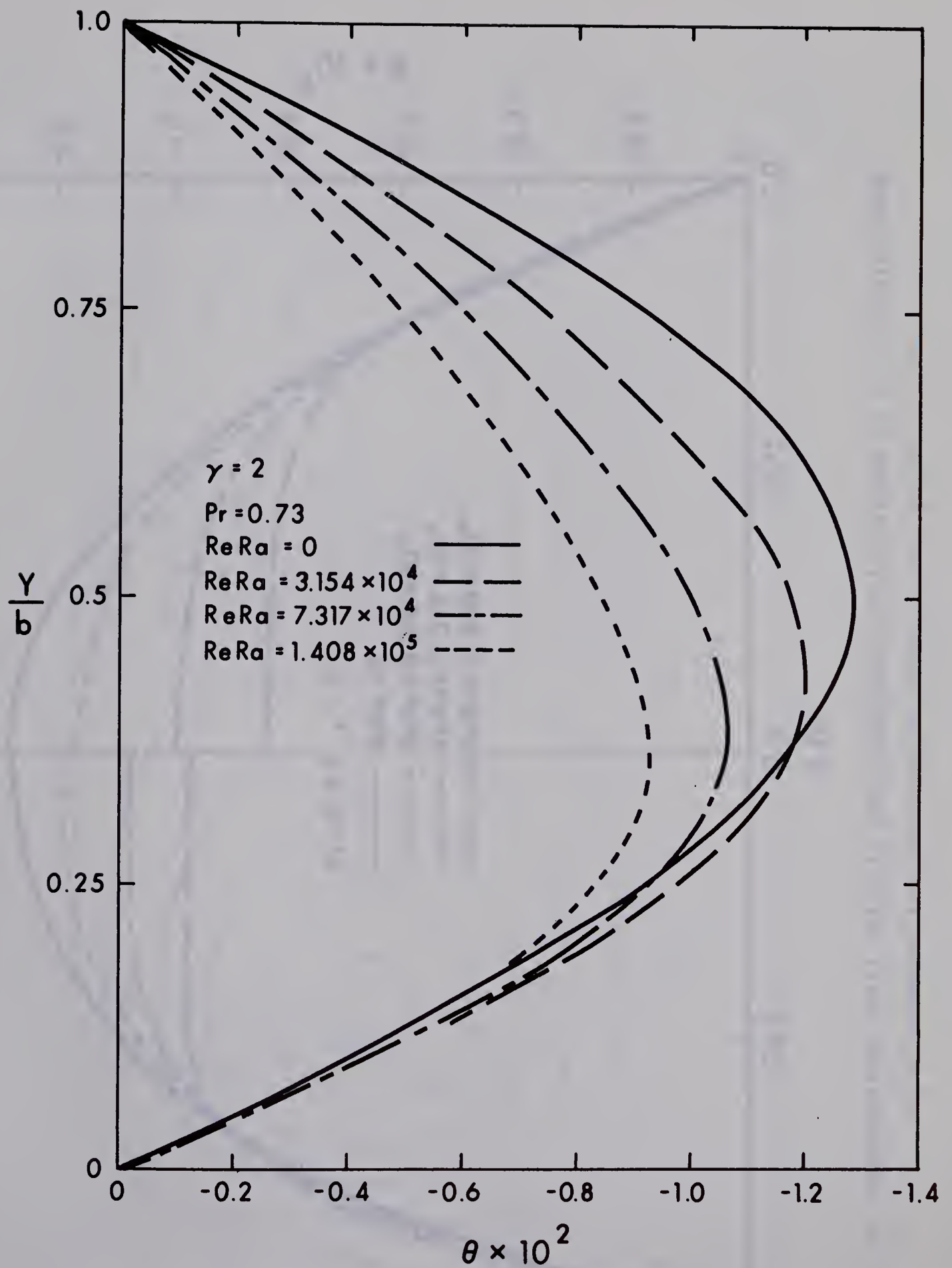


Fig. 8 Dimensionless Temperature Distribution at $X = a/2$ With $ReRa$ as a Parameter in a Rectangular Channel $\gamma = 2$ and $Pr = 0.73$

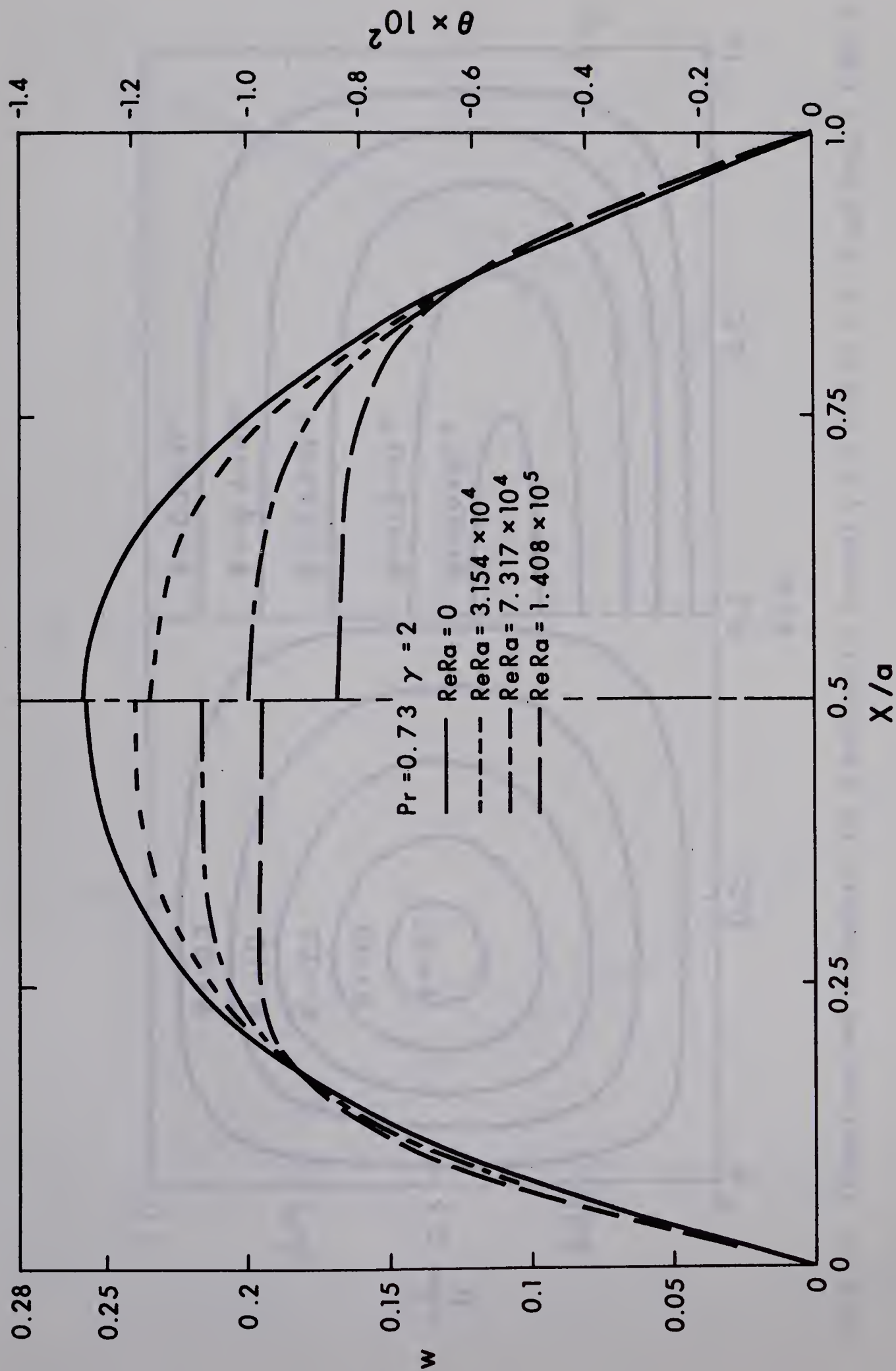


Fig. 9 Dimensionless Axial Velocity and Temperature Distributions at $Y = b/2$ With $ReRa$ As a Parameter in a Rectangular Channel $\gamma = 2$ and $Pr = 0.73$

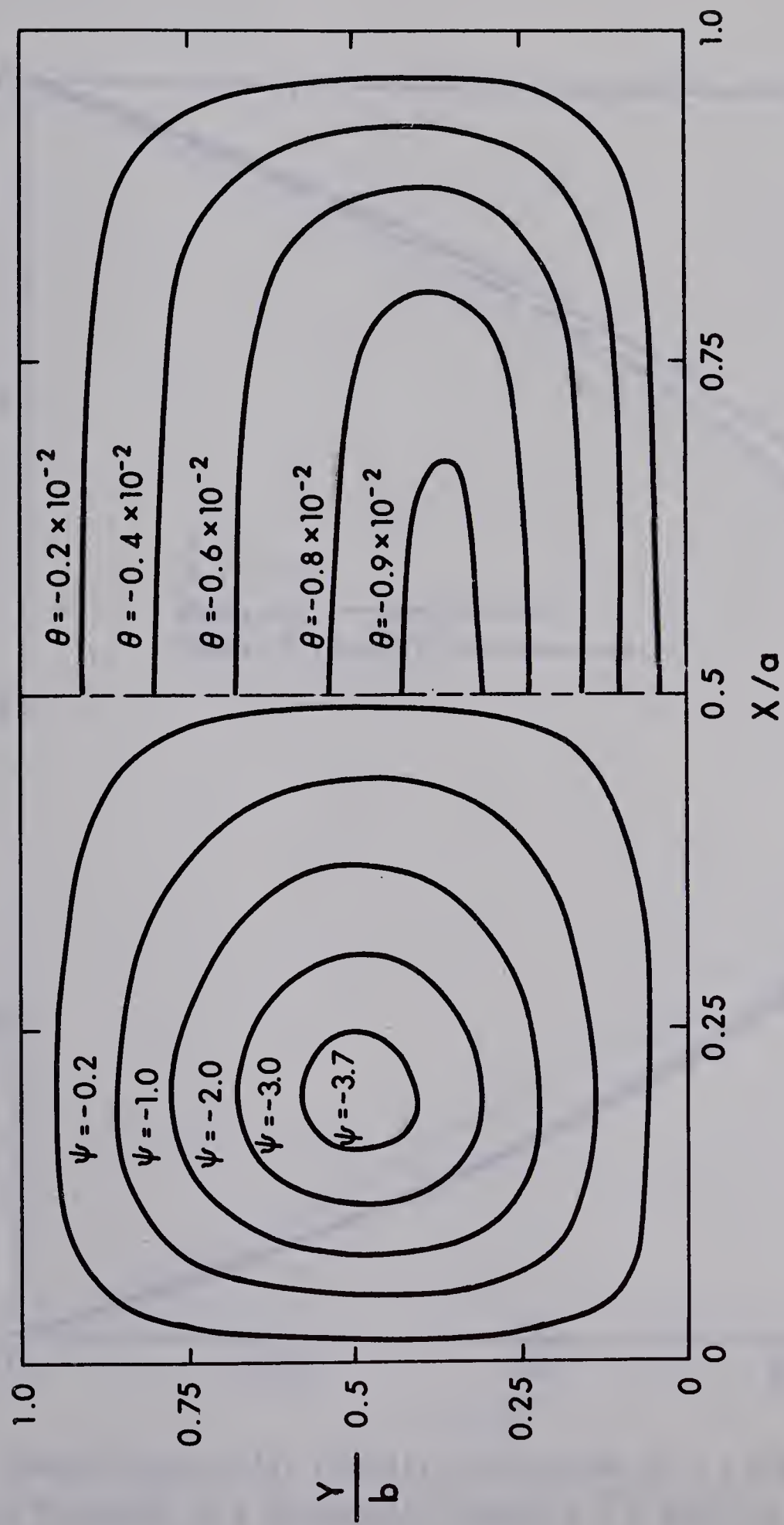


Fig. 10 Streamlines and Isotherms for a Rectangular Channel $\gamma = 2$ With $Pr = 0.73$ and $ReRa = 1.408 \times 10^5$

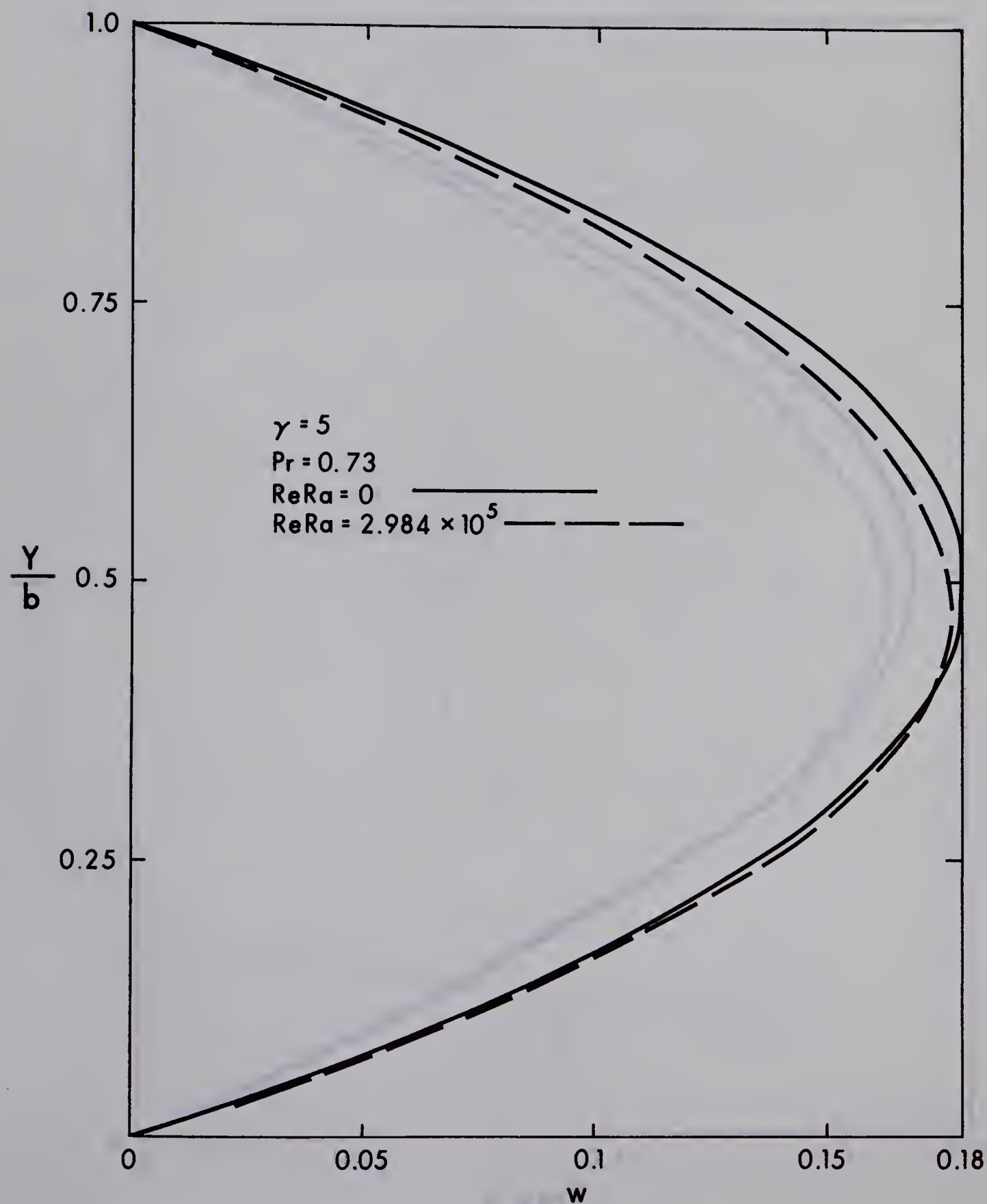


Fig. 11 Dimensionless Axial Velocity Distribution at $X = a/2$ With $ReRa$ as a Parameter in a Rectangular Channel $\gamma = 5$ and $Pr = 0.73$

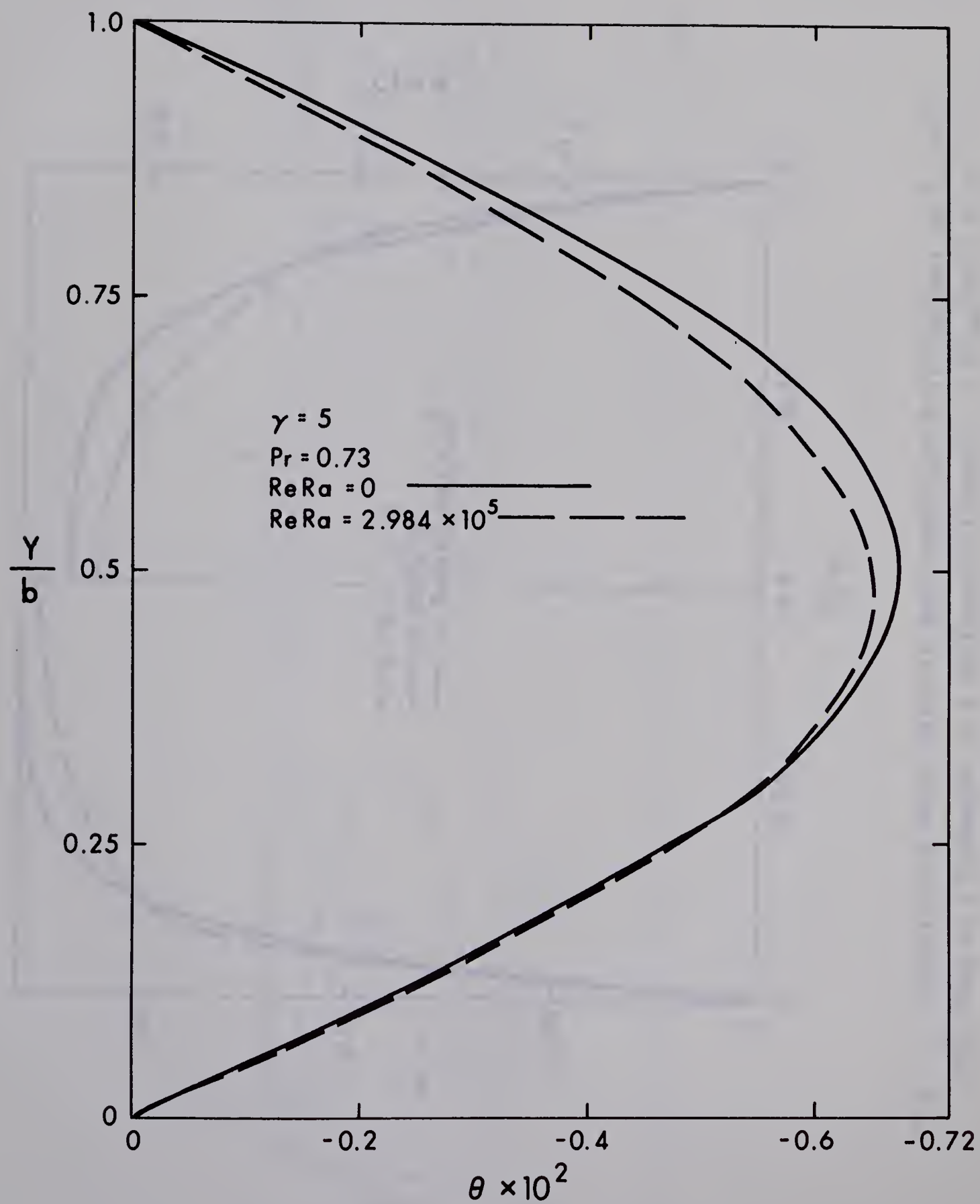


Fig. 12 Dimensionless Temperature Distribution at $X = a/2$ With $ReRa$ as a Parameter in a Rectangular Channel $\gamma = 5$ and $Pr = 0.73$

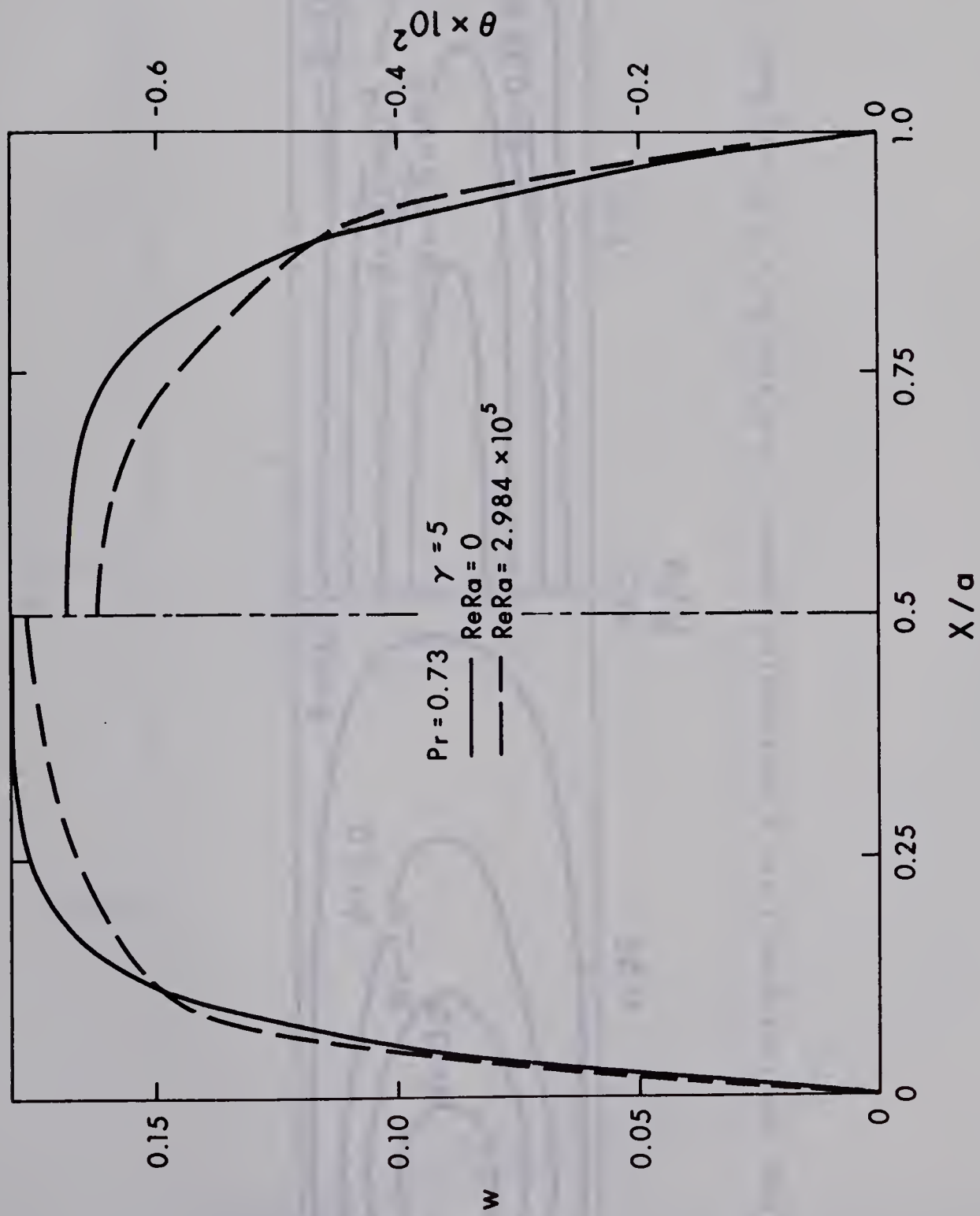


Fig. 13 Dimensionless Axial Velocity and Temperature Distributions at $Y = b/2$ With $ReRa$ as a Parameter in a Rectangular Channel $\gamma = 5$ and $Pr = 0.73$

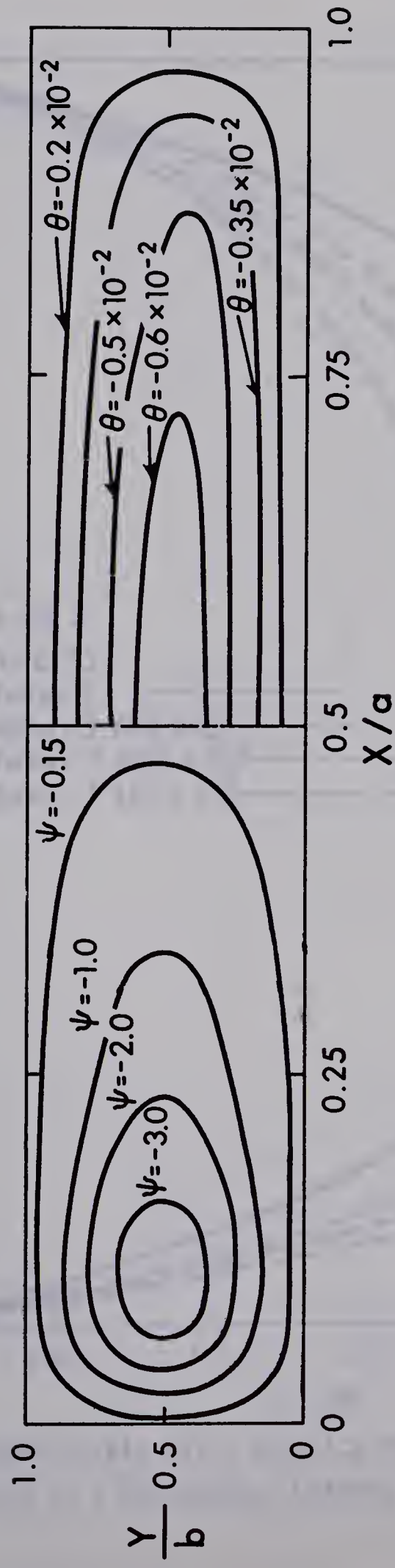


Fig. 14 Streamlines and Isothermals for a Rectangular Channel $\gamma = 5$ With $Pr = 0.73$ and $ReRa = 2.984 \times 10^5$

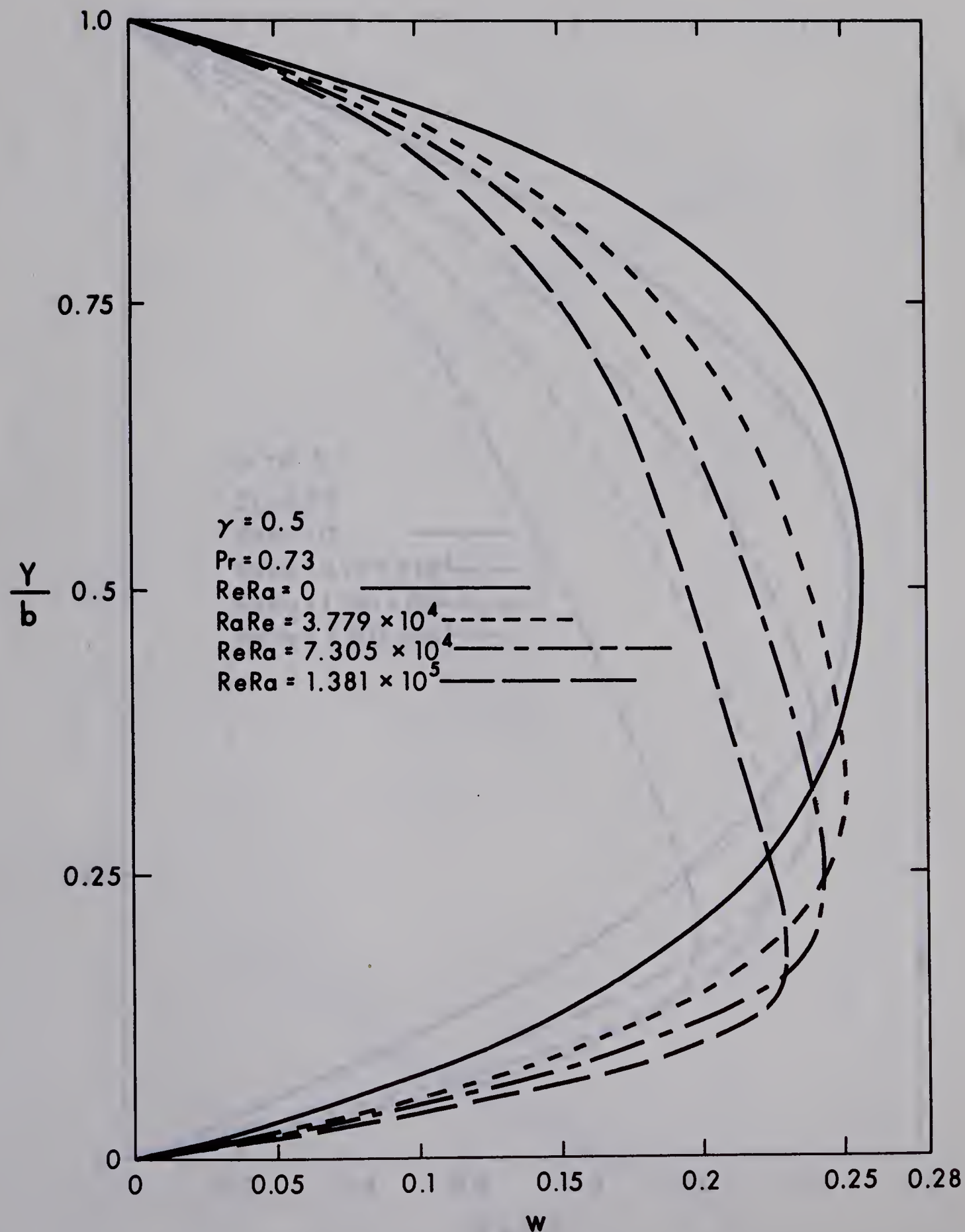


Fig. 15 Dimensionless Axial Velocity Distribution at $X = a/2$ With $ReRa$ as a Parameter in a Rectangular Channel $\gamma = 0.5$ and $Pr = 0.73$

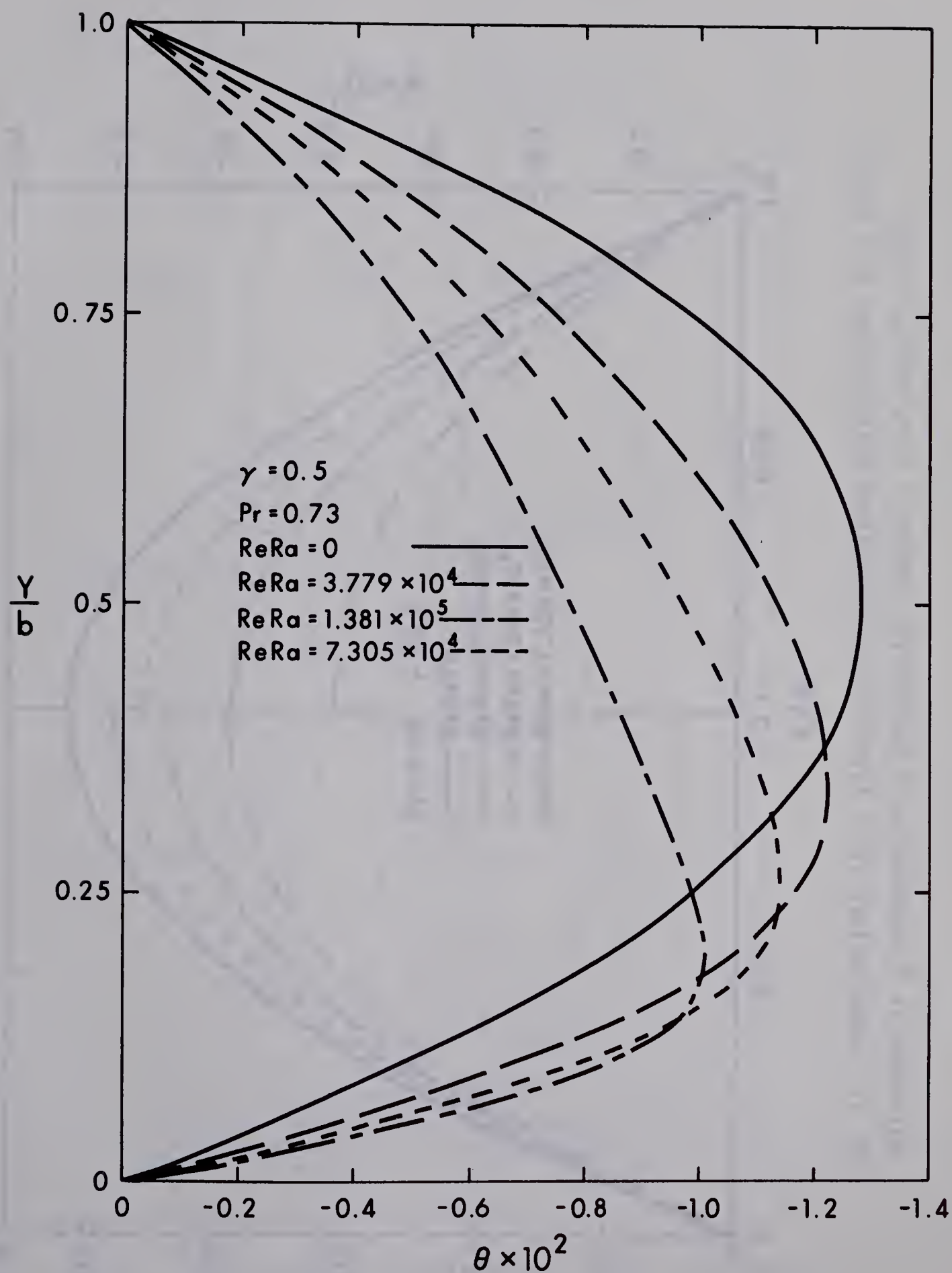


Fig. 16 Dimensionless Temperature Distribution at $X = a/2$ With $ReRa$ as a Parameter in a Rectangular Channel $\gamma = 0.5$ and $Pr = 0.73$

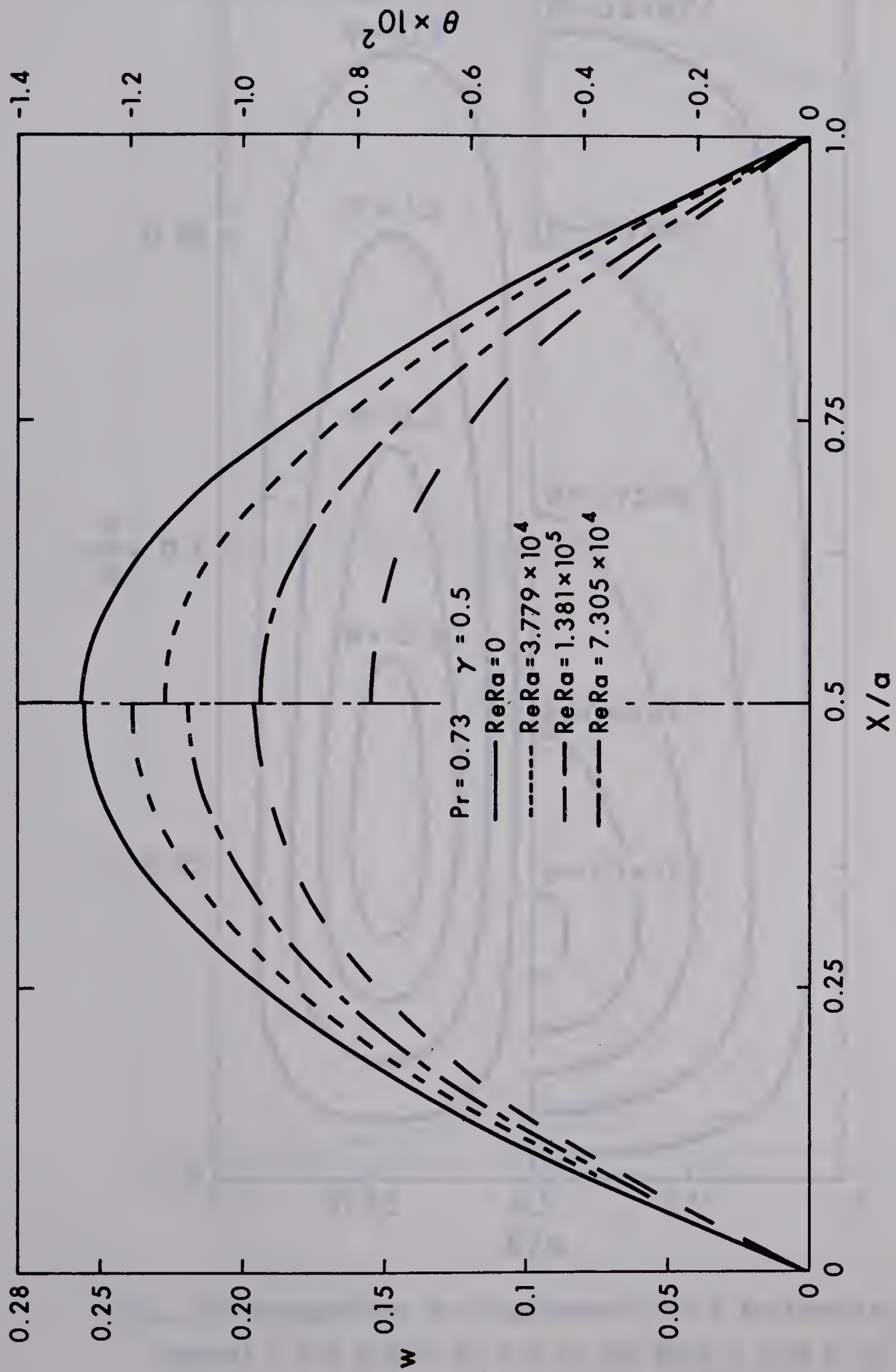


Fig. 17 Dimensionless Axial Velocity and Temperature Distributions at $Y = b/2$
 With $ReRa$ as a Parameter in a Rectangular Channel $\gamma = 0.5$ and $Pr = 0.73$

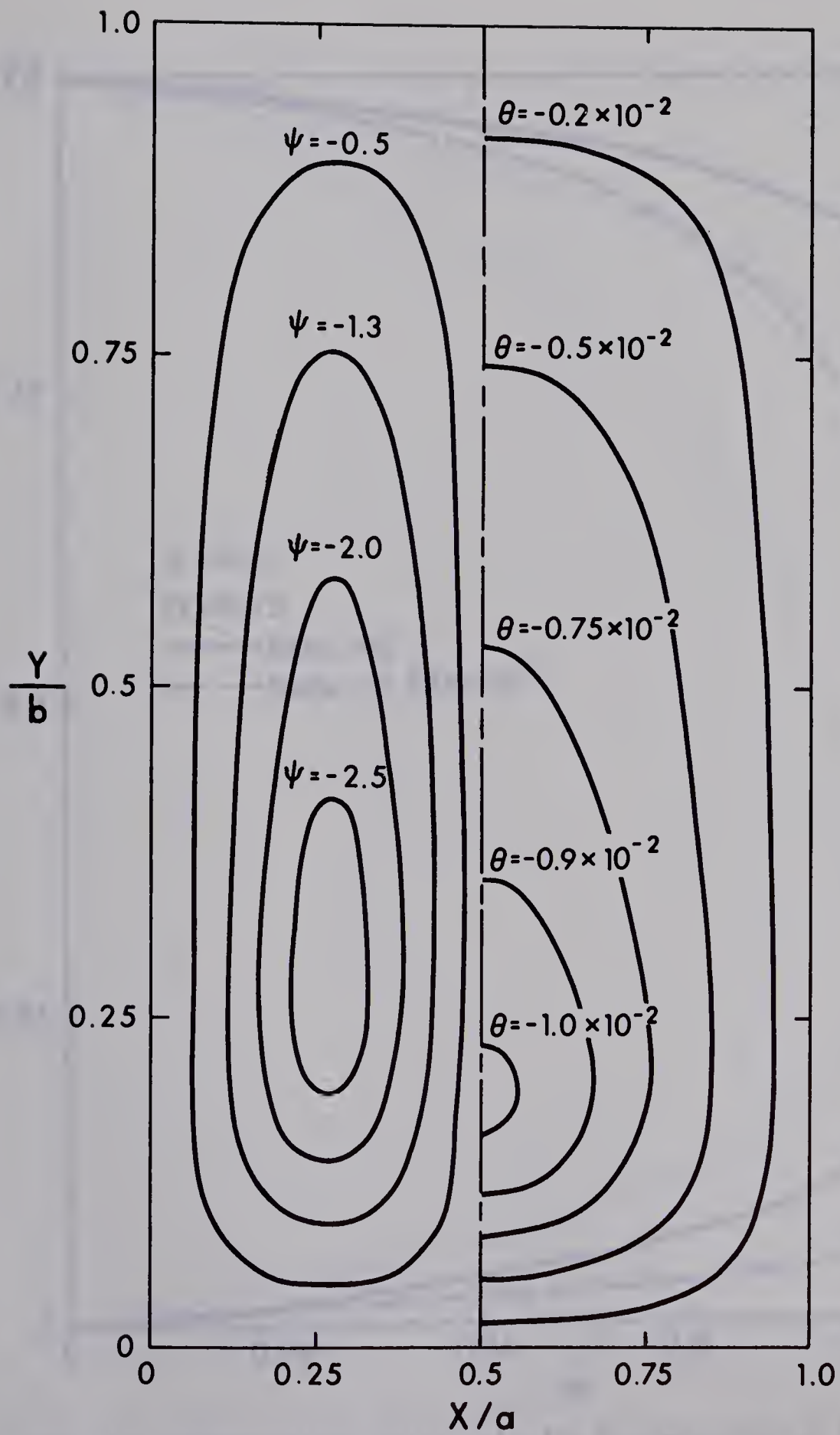


Fig. 18 Streamlines and Isotherms for a Rectangular Channel $\gamma = 0.5$ With $Pr = 0.73$ and $ReRa = 1.38 \times 10^5$

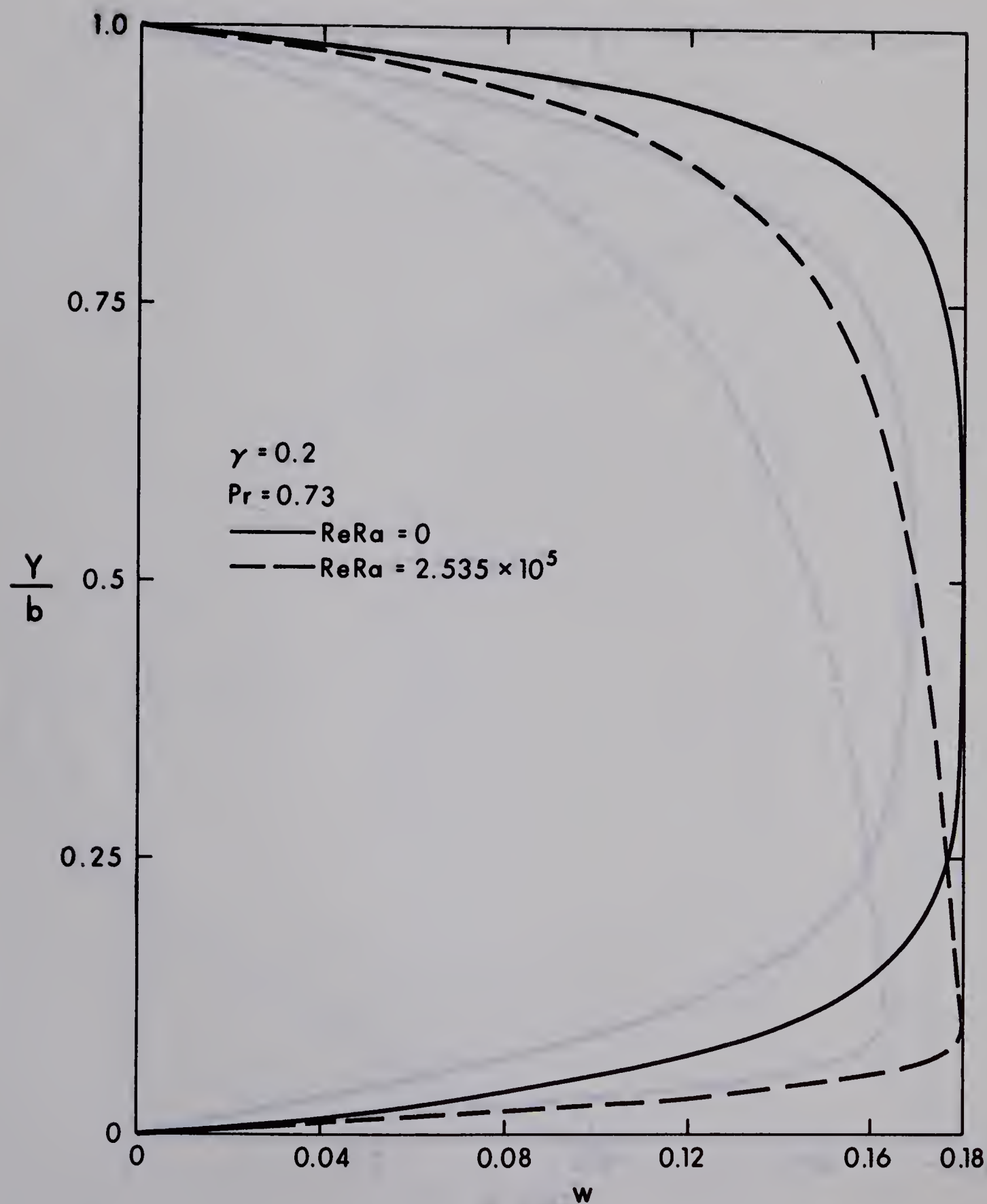


Fig. 19 Dimensionless Axial Velocity Distribution at $X = a/2$ With $ReRa$ as a Parameter in a Rectangular Channel $\gamma = 0.2$ and $Pr = 0.73$

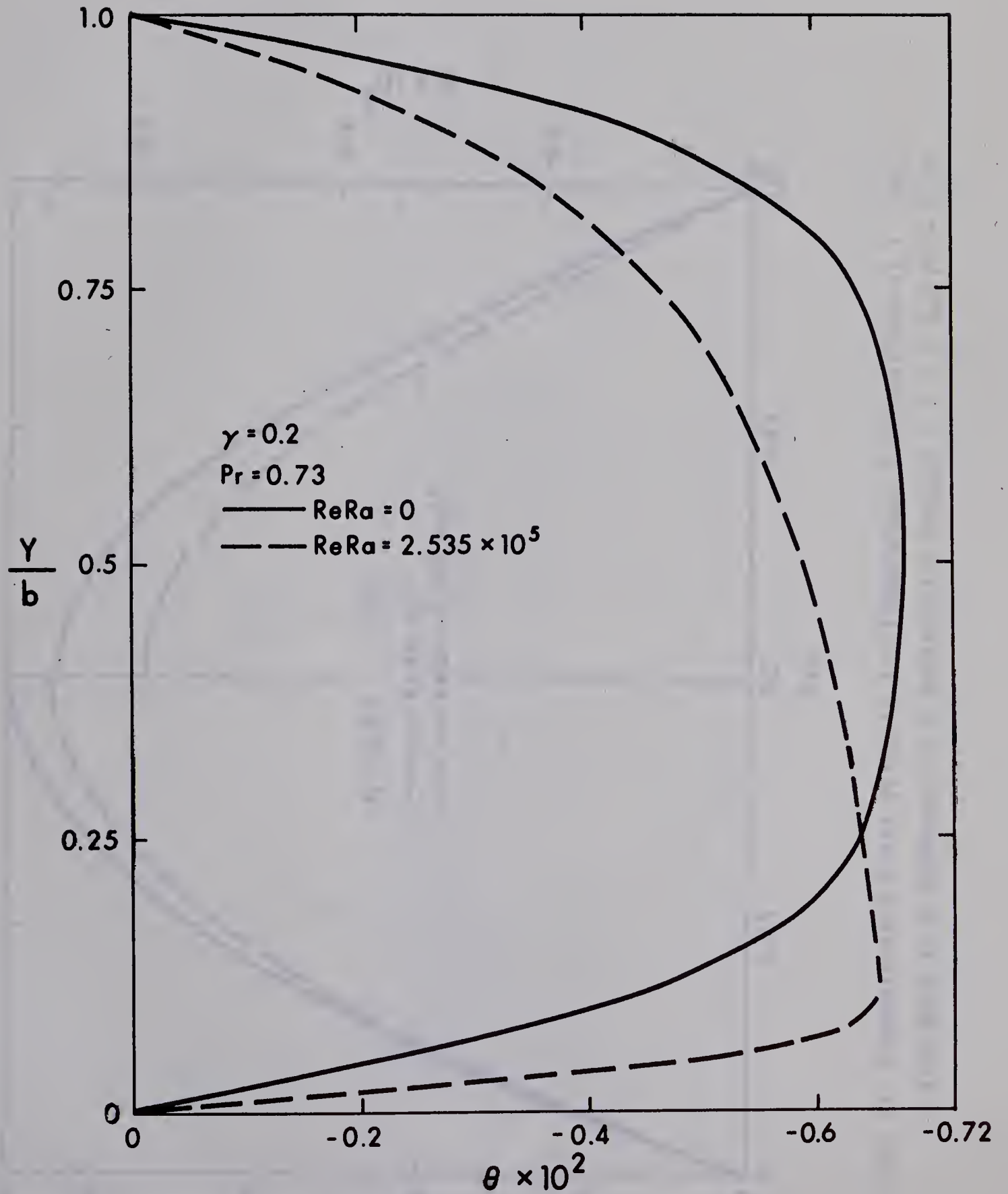


Fig. 20 Dimensionless Temperature Distribution at $X = a/2$ With $ReRa$ As a Parameter in a Rectangular Channel $\gamma = 0.2$ and $Pr = 0.73$

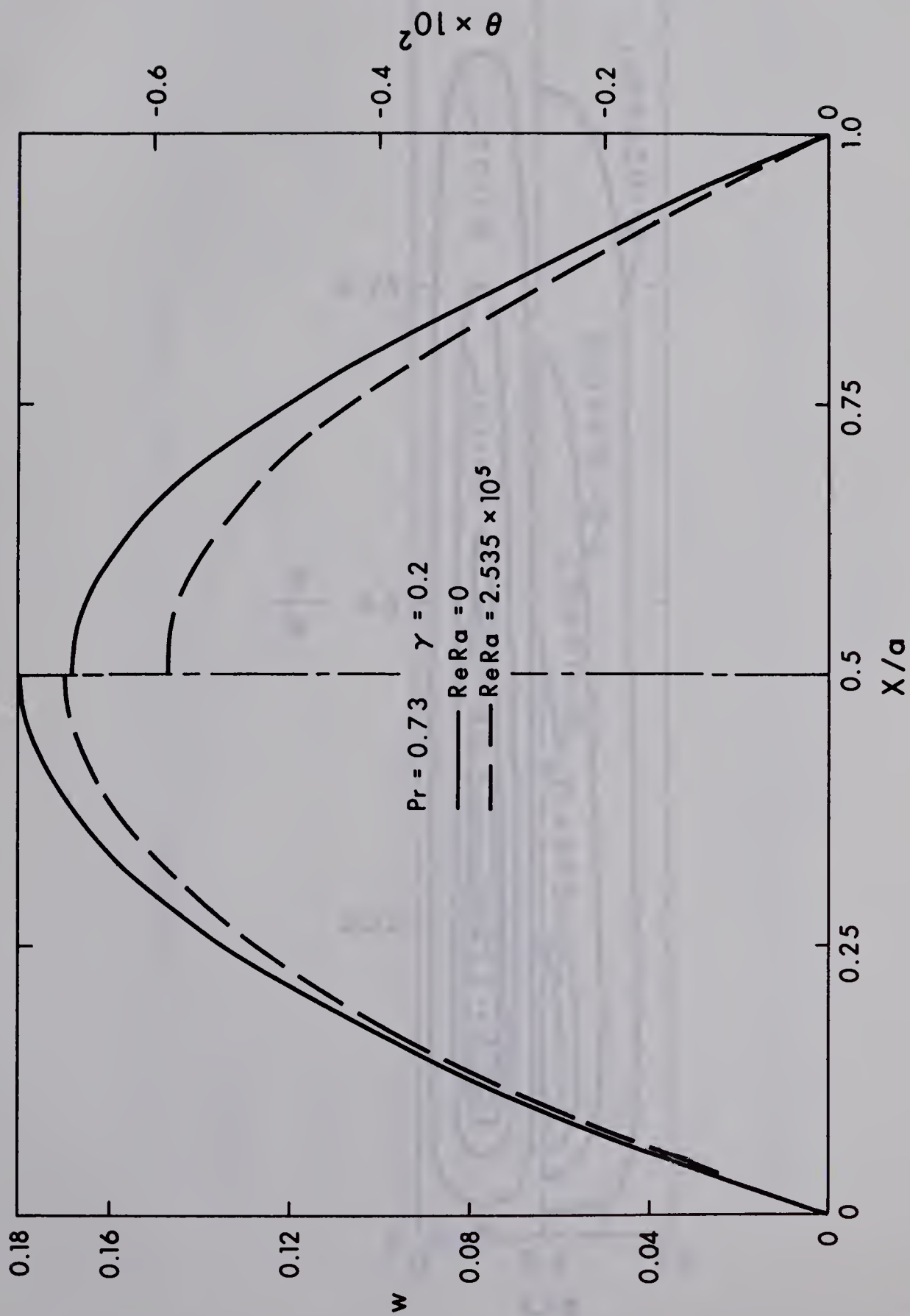


Fig. 21 Dimensionless Axial Velocity and Temperature Distributions at $\gamma = b/2$
 With $ReRa$ as a Parameter in a Rectangular Channel $\gamma = 0.2$ and $Pr = 0.73$

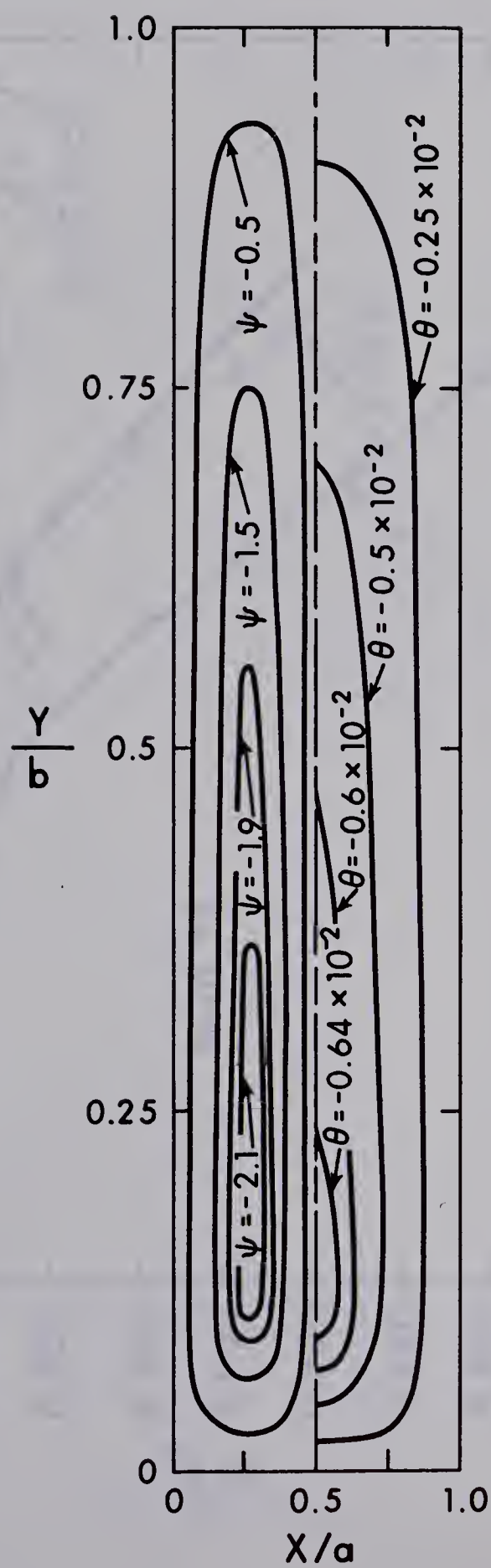


Fig. 22 Streamlines and Isotherms for a Rectangular Channel
 $\gamma = 0.2$ With $Pr = 0.73$ and $ReRa = 2.535 \times 10^5$

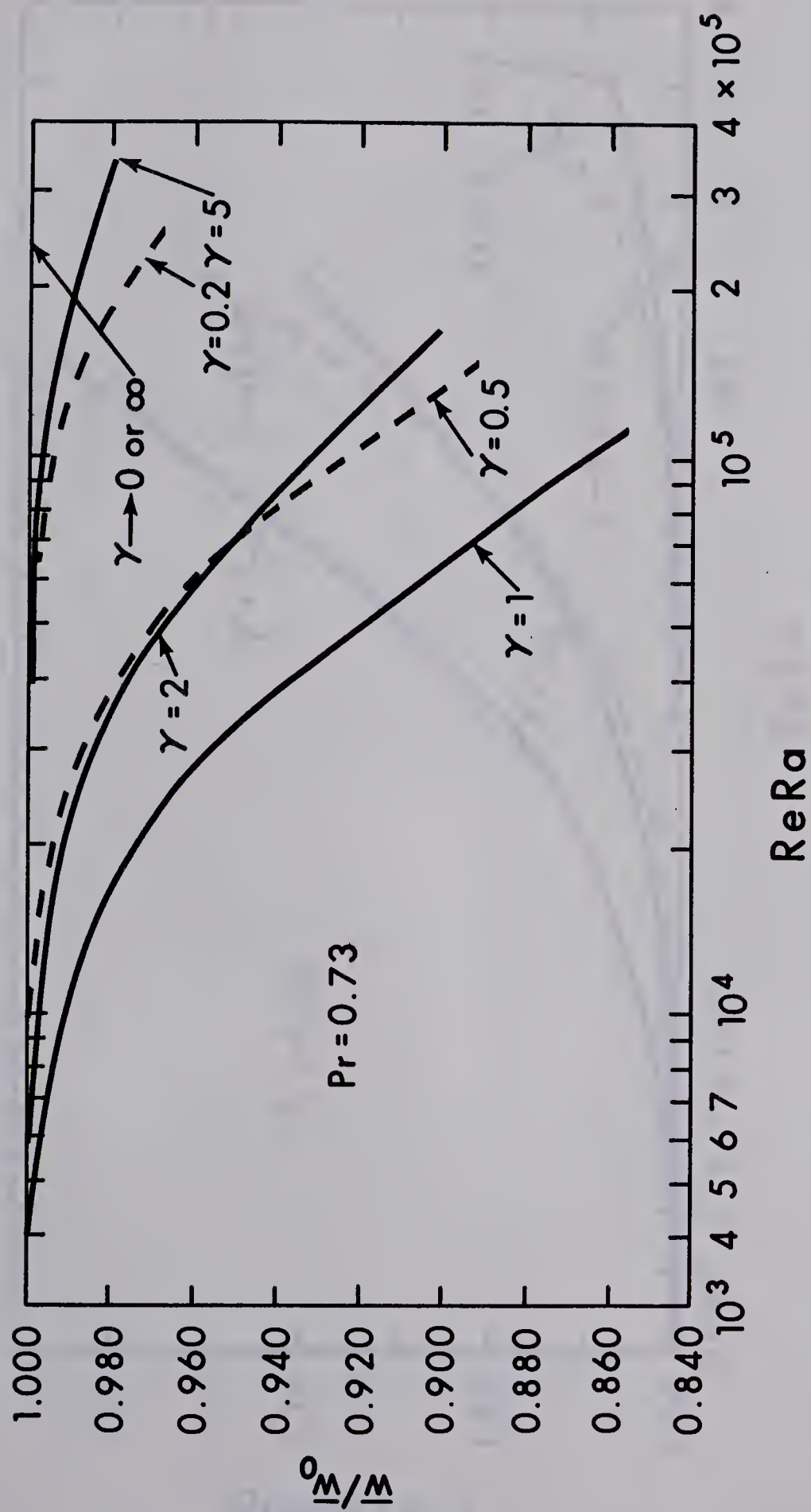


Fig. 23 $\frac{w}{w_0}$ Versus $ReRa$ With Aspect Ratio γ as a Parameter

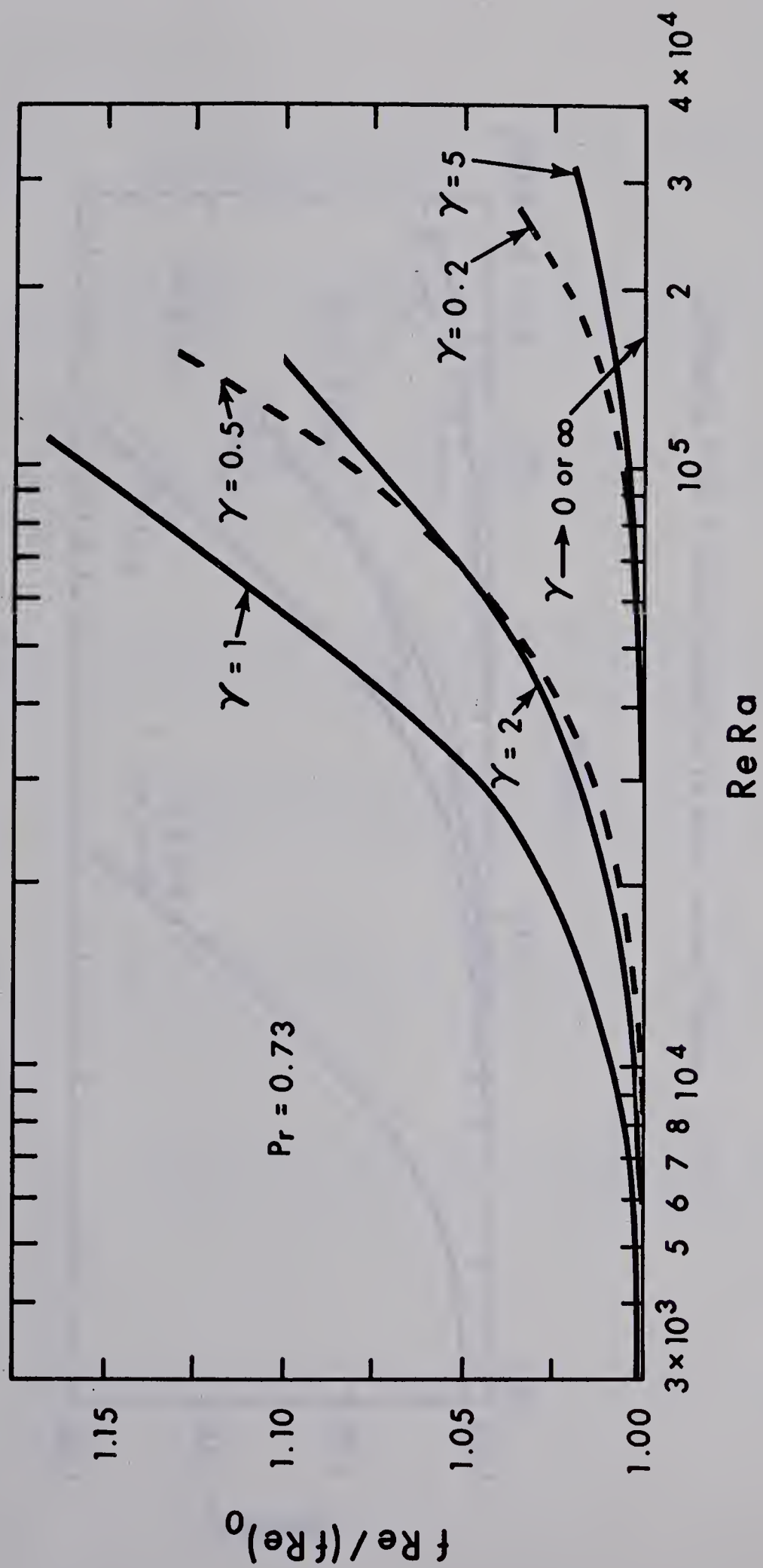


Fig. 24 $f Re / (f Re)_0$ With Aspect Ratio γ as a Parameter

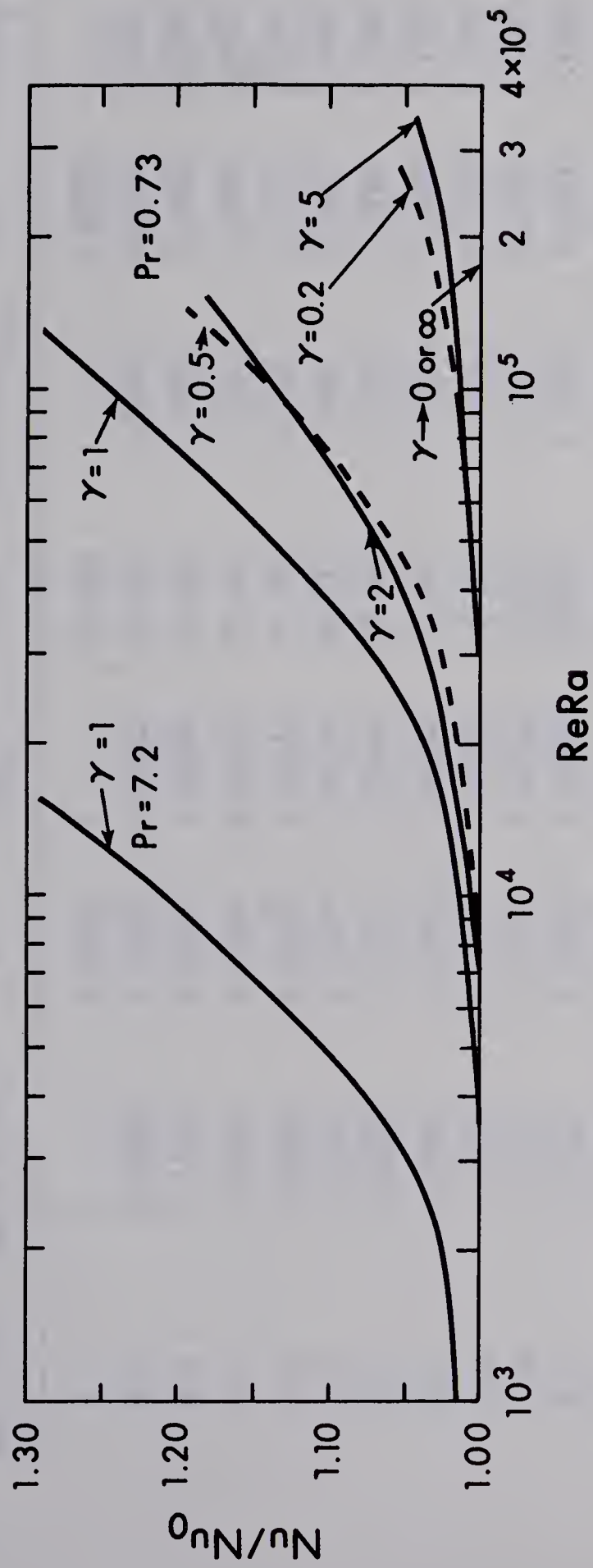


Fig. 25 Nu/Nu_0 Versus $ReRa$ With Aspect Ratio γ as a Parameter

Table 1 Numerical Results for Square Channel $\gamma = 1$ and $Pr = 0.73$

$Ra_C \times 10^{-5}$	$RaRe \times 10^{-4}$	\bar{w}	\bar{w}/\bar{w}_0	$f \cdot Re$	$fRe/(fRe)_0$	Nu	Nu/Nu_0
0	0	0.14045	1	14.204	1	3.6085	1
0.5	0.69960	0.13992	0.99623	14.259	1.0039	3.6304	1.0061
0.8	1.1133	0.13917	0.99089	14.336	1.0093	3.6593	1.0141
1.0	1.3855	0.13855	0.98647	14.399	1.0137	3.6833	1.0207
1.5	2.0523	0.13682	0.97415	14.581	1.0265	3.7516	1.0397
2.0	2.7008	0.13504	0.96148	14.773	1.0401	3.8263	1.0604
3.0	3.9528	0.13176	0.93813	15.140	1.0659	3.9720	1.1007
4.0	5.1608	0.12902	0.91862	15.461	1.0885	4.1043	1.1374
4.5	5.7524	0.12783	0.91015	15.604	1.0986	4.1645	1.1541
5.0	6.3375	0.12675	0.90246	15.737	1.1079	4.2210	1.1697
6.0	7.4904	0.12484	0.88886	15.977	1.1248	4.3241	1.1983
6.5	8.0594	0.12399	0.88281	16.086	1.1325	4.3713	1.2114
7.5	9.1853	0.12247	0.87198	16.285	1.1465	4.4581	1.2354
8.0	9.7432	0.12179	0.86714	16.376	1.1529	4.4984	1.2466
8.5	10.298	0.12115	0.86258	16.462	1.1590	4.5371	1.2573
9.0	10.849	0.12054	0.85824	16.545	1.1648	4.5736	1.2675

Table 2 Numerical Results for Square Channel $\gamma = 1$ and $Pr = 7.2$

$RaC \times 10^{-5}$	$RaRe \times 10^{-4}$	\bar{w}	\bar{w}/\bar{w}_0	$f \cdot Re$	$fRe/(fRe)_0$	Nu	Nu/Nu_0
0	0	0.14045	1	14.204	1	3.6085	1
0.1	0.14043	0.14043	0.99986	14.207	1.0002	3.6563	1.0133
0.2	0.28076	0.14038	0.99950	14.212	1.0006	3.7640	1.0431
0.3	0.42090	0.14030	0.99893	14.220	1.0011	3.8908	1.0782
0.4	0.56088	0.14022	0.99836	14.228	1.0017	4.0157	1.1128
0.5	0.70065	0.14013	0.99772	14.237	1.0023	4.1313	1.1449
0.6	0.84024	0.14004	0.99708	14.246	1.0030	4.2370	1.1742
0.8	1.1189	0.13986	0.99580	14.264	1.0042	4.4218	1.2254
1.0	1.3969	0.13969	0.99459	14.282	1.0055	4.5770	1.2684
1.1	1.5357	0.13961	0.99402	14.291	1.0065	4.6424	1.2865

Table 3 Numerical Results for Aspect Ratio $\gamma = 2$ and $Pr = 0.73$

$RaC \times 10^{-5}$	$RaRe \times 10^{-4}$	\bar{w}	\bar{w}/\bar{w}_0	$f \cdot Re$	$fRe/(fRe)_0$	Nu	Nu/Nu_0
0	0	0.12851	1	15.517	1	4.1251	1
0.5	0.64190	0.12838	0.99899	15.533	1.0010	4.1339	1.0021
0.8	1.0254	0.12818	0.99743	15.557	1.0026	4.1449	1.0048
1.0	1.2801	0.12801	0.99611	15.578	1.0039	4.1546	1.0072
1.5	1.9120	0.12749	0.99206	15.643	1.0081	4.1852	1.0146
2.0	2.5368	0.12684	0.98700	15.721	1.0131	4.2220	1.0235
2.5	3.1543	0.12617	0.98179	15.805	1.0186	4.2617	1.0331
3.8	4.7291	0.12445	0.96841	16.022	1.0325	4.3660	1.0584
4.5	5.5615	0.12359	0.96172	16.133	1.0397	4.4195	1.0714
6.0	7.3170	0.12195	0.94895	16.349	1.0536	4.5254	1.0970
7.5	9.0413	0.12055	0.93806	16.538	1.0658	4.6180	1.1195
9.0	10.739	0.11932	0.92849	16.707	1.0767	4.6998	1.1393
10.0	11.859	0.11859	0.92281	16.809	1.0833	4.7494	1.1513
11.0	12.971	0.11792	0.91759	16.904	1.0894	4.7952	1.1624
12.0	14.076	0.11730	0.91277	16.994	1.0952	4.8386	1.1730
13.0	15.172	0.11671	0.90818	17.086	1.1011	4.8792	1.1828

Table 4 Numerical Results for Aspect Ratio $\gamma = 5$ and $Pr = 0.73$

$RaC \times 10^{-5}$	$RaRe \times 10^{-4}$	\bar{w}	\bar{w}/\bar{w}_0	$f \cdot Re$	$fRe/(fRe)_0$	Nu	Nu/Nu_0
0	0	0.10482	1	19.046	1	5.7407	1
1.0	1.0482	0.10482	1.0000	19.047	1.0001	5.7422	1.0003
1.5	1.5720	0.10480	0.99981	19.048	1.0001	5.7429	1.0004
2.2	2.3056	0.10480	0.99981	19.050	1.0002	5.7443	1.0006
2.9	3.0390	0.10478	0.99962	19.053	1.0004	5.7461	1.0009
6.0	6.2790	0.10465	0.99838	19.077	1.0016	5.7594	1.0033
11.0	11.475	0.10432	0.99523	19.136	1.0047	5.7932	1.0092
15.0	15.602	0.10401	0.99227	19.193	1.0077	5.8252	1.0147
21.0	21.741	0.10353	0.98769	19.280	1.0123	5.8744	1.0233
25.0	25.805	0.10322	0.98474	19.338	1.0153	5.9066	1.0289
29.0	29.844	0.10291	0.98178	19.395	1.0183	5.9377	1.0343
32.0	32.861	0.10269	0.97968	19.437	1.0205	5.9602	1.0382

Table 5 Numerical Results for Aspect Ratio $\gamma = 0.5$ and $Pr = 0.73$

$RaC \times 10^{-5}$	$RaRe \times 10^{-4}$	\bar{w}	\bar{w}/\bar{w}_0	$f \cdot Re$	$fRe/(fRe)_0$	Nu	Nu/Nu_0
0	0	0.12851	1	15.517	1	4.1252	1
1.0	1.2817	0.12817	0.99735	15.558	1.0026	4.1460	1.0050
1.6	2.0427	0.12767	0.99346	15.618	1.0065	4.1738	1.0118
2.0	2.5450	0.12725	0.99020	15.670	1.0099	4.1977	1.0176
3.0	3.7794	0.12598	0.98031	15.826	1.0203	4.2690	1.0349
4.0	4.9828	0.12457	0.96934	16.003	1.0313	4.3476	1.0539
5.0	6.1565	0.12313	0.95814	16.187	1.0432	4.4278	1.0734
6.0	7.3050	0.12175	0.94740	16.369	1.0549	4.5064	1.0924
7.5	8.9850	0.11980	0.93222	16.630	1.0717	4.6183	1.1195
9.0	10.625	0.11805	0.91861	16.872	1.0873	4.7218	1.1446
11.0	12.758	0.11598	0.90250	17.167	1.1063	4.8470	1.1750
12.0	13.806	0.11505	0.89526	17.302	1.1150	4.9050	1.1890
12.5	14.325	0.11460	0.89176	17.367	1.1192	4.9328	1.1958

Table 6 Numerical Results for Aspect Ratio $\gamma = 0.2$ and $Pr = 0.73$

$RaC \times 10^{-5}$	$RaRe \times 10^{-4}$	\bar{w}	\bar{w}/\bar{w}_0	$f \cdot Re$	$fRe/(fRe)_0$	Nu	Nu/Nu_0
0	0	0.10482	1	19.046	1	5.7401	1
1.0	1.0482	0.10482	1.0000	19.047	1.0001	5.7423	1.0004
1.5	1.5721	0.10481	0.99990	19.049	1.0002	5.7432	1.0005
5.0	5.2320	0.10464	0.99828	19.078	1.0017	5.7592	1.0033
6.3	6.5860	0.10454	0.99733	19.097	1.0027	5.7691	1.0051
8.0	8.3496	0.10437	0.99571	19.128	1.0043	5.7849	1.0078
10.0	10.412	0.10412	0.99332	19.172	1.0066	5.8069	1.0116
15.0	15.500	0.10333	0.98579	19.315	1.0141	5.8736	1.0233
20.0	20.478	0.10239	0.97682	19.487	1.0232	5.9493	1.0365
25.0	25.348	0.10139	0.96728	19.672	1.0329	6.0276	1.0501
26.0	26.309	0.10119	0.96537	19.709	1.0348	6.0433	1.0528

Table 7 Comparison of Nusselt Number with Exact Value [20] for ReRa = 0

γ	0.2	0.5	1	2	5
Exact	5.7376	4.1245	3.6080	4.1245	5.7376
This Work	5.7401	4.1252	3.6085	4.1251	5.7407
M,N	8,80	10,40	16,32	20,20	40,16

Table 8 Numerical Results of $\overline{(\frac{\partial w}{\partial n})_W}$, $|\frac{\partial \theta}{\partial n}|_W$ and $w/4$ for Pr = 0.73

γ	0.2	0.5	1	2	5
ReRa $\times 10^{-4}$	26.309	14.325	10.849	15.172	32.861
$\overline{(\frac{\partial w}{\partial n})_W}$	0.99716	0.99515	0.99717	0.99711	0.99799
$ \frac{\partial \theta}{\partial n} _W \times 10$	0.25371	0.28675	0.30175	0.29257	0.25773
$\overline{\frac{w}{4}} \times 10$	0.25297	0.28650	0.30135	0.29177	0.25672

Note: The above values represent the greatest deviation from equation (38). For the case $\gamma = 1$, Pr = 7.2, the differences are less than the case with Pr = 0.73 for the same aspect ratio.

